Table I Number of surviving blastocysts and the mean oxygen consumption of their ICM and TE sides.

	Hours after warming						
	1.5	3	4.5	6	7.5	9	24
No. surviving (%)	44 (100)	44 (100)	44 (100)	33 (75)	30 (68)	30 (68)	28 (64)
ICM side	3.9 (29)	4.7 (36)	5.6 (38)	6.3 (31)	7.1 (28)	7.8 (28)	9.7 (25)
TE side	4.1 (29)	4.9 (36)	5.8 (38)	6.7 (31)	7.3 (28)	7.9 (28)	10.2 (25)

Oxygen consumption is expressed as fmol/s/blastocyst (no. of blastocysts).
If the ICM was clearly discernible, the oxygen consumption of the TE adjacent to ICM (ICM side) and TE far from ICM (TE side) was measured. There were no significant differences in oxygen consumption between the points near and far from the ICM.

increasing concentrations of ethanol and embedded in epoxy resins. Ultrathin sections were stained with uranyl acetate and examined using transmission electron microscopy (JEM-1011; JEOL, Tokyo, Japan).

Statistical analysis

BQS and oxygen consumption data were analysed using analysis of variance (ANOVA) followed by the Tukey–Kramer test. The relationship between the blastocyst cell number and blastocyst oxygen consumption at 24 h was analysed using the correlation coefficient (r). P-values of <0.05 were considered significant. Data are represented as mean ± SEM. Statistical analysis was performed using StatView version 5 (SAS Institute Inc., Cary, NC, USA).

Results

All blastocysts survived after cryopreservation. Of these, 32 shrank just after warming (0 h, 72.7%); however, all embryos re-formed blastocoels at 1.5 h after warming. As shown in Table I, there were no differences in the oxygen consumption between the TE side and ICM side at any measurement times. Subsequently, the oxygen consumption of the ICM side was treated the same as that of the TE side.

At 24 h after culture, the numbers of blastocysts in the hatched, hatching, arrested and degenerated groups were 8 (18%), 12 (27%), 8 (18%) and 16 (36%), respectively. The survival rate at 24 h after culture was 63.6%. There were no significant differences in the BQSs of these groups until 4.5 h, as shown in Fig. 1. However, the BQS in the degenerated group was significantly ($P < 0.05$) less than in the hatched group from 6 h onwards and the BQS in the arrested group was significantly lower than in the hatched group from 7.5 h onwards ($P < 0.05$), whereas the BQS of the hatching group was only significantly less than the hatched group at 24 h.

Oxygen consumptions (mean ± SEM, fmol/s) of all vitrified-warmed blastocysts just after warming [0 h, 2.4 ± 0.1 ($n = 44$) were significantly lower ($P < 0.05$) than those of non-vitrified blastocysts (7.8 ± 0.3 ($n = 10$; Fig. 2)]. There was no difference in oxygen consumption among the four groups at 0 h. The oxygen consumption of blastocysts in the hatched group increased with time and was significantly higher ($P < 0.05$) at 7.5 and 9 h than in the hatching group, and from 1.5 h onwards than in the arrested group and in the degenerated group. Blastocysts in the degenerated group also showed an increase in oxygen consumption until 4.5 h. Once morphological degeneration was observed at 6 h, the oxygen consumption decreased drastically and fell to 1.8 ± 0.5 fmol/s ($n = 16$) at 24 h.

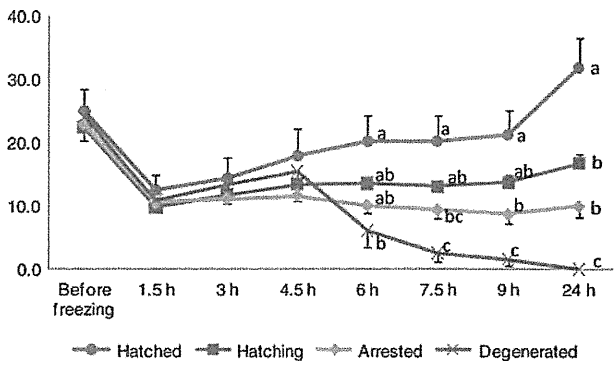

Figure 1 Blastocyst quality scores (BQS) before and after cryopreservation. BQS is defined as the product of the degree of expansion and hatching status and ICM and TE grades. Values with different superscripts at the same observation time are significantly different ($^{abc}P < 0.05$, One-way ANOVA with Tukey–Kramer test). Data are represented as mean ± SEM. There were no significant differences in BQS among groups at each observation time until 4.5 h.

There was a correlation between the cell number of the surviving blastocysts (hatched, hatching and arrested groups; 28 samples) and their oxygen consumption at 24 h ($r^2 = 0.44$, $P < 0.01$). Mitochondrial CCO activity was detected in blastocysts at 24 h after warming, but not at 0 h (Fig. 3).

Discussion

The results of the present study indicate that the oxygen consumption rate of blastocysts just after warming was significantly lower than that of fresh blastocysts. The oxygen consumption rate of blastocysts increased with time after warming. Blastocysts that retained high developmental competence recovered rapidly compared with those in other groups. Moreover, mitochondrial CCO activity was not observed at 0 h after warming, but was observed at 24 h. These data suggest that mitochondrial functions are restrained or obstructed somewhere during the cryopreservation process. The freezing process has been shown to induce damage to membranes and cristae in mitochondria of bovine embryos (Mohr and Trounson, 1981); however, broken membranes were not detected in the present experiments. Furthermore, the oxygen uptake by vitrified bovine blastocysts at 18 h after thawing was identical to that of non-vitrified blastocysts

(Kaidi *et al.*, 2001). In this study, after 6 h the oxygen consumption rate of vitrified and warmed human blastocysts in the hatched group had recovered to that exhibited by fresh blastocysts.

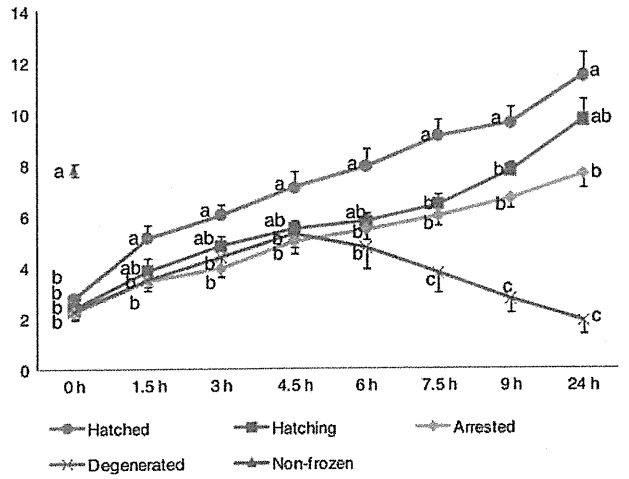

Figure 2 Change in mean oxygen consumption (fmol/s) of vitrified-warmed blastocysts over time. Data are represented as mean ± SEM. Values with different superscripts at the same observation time are significantly different ($^{abc}P < 0.05$, One-way ANOVA with Tukey–Kramer test).

Oxygen consumption at the ICM and TE sides were almost identical (Table I). This contrasts with animal studies, in mice, the TE consumed significantly more oxygen, produced more ATP and contained a greater number of mitochondria than the ICM (Houghton, 2006). Amino acid turnover was also significantly greater in the TE than in the ICM. When compared with ICM, TE was believed to produce ~80% of the ATP generated. Furthermore, the TE had higher pyruvate and lower glucose consumption than did the ICM in cattle (Gopichandran and Leese, 2003). Based on the above evidence, the ICM of human blastocysts was believed to display a relatively lower TCA cycle activity than those of the TE. However, even when the electrode is over the ICM, it is likely to measure the oxygen consumption of the surrounding TE and there is no reason to suppose that the TE adjacent to the ICM has a different metabolic rate than in other regions.

In this study, we observed an increase in the oxygen consumption rate of blastocysts with culture time after warming. In particular, the respiration values of blastocysts in the hatched group recovered promptly when compared with those in the other groups. Oxygen consumption was highly dependent on developmental competence regardless of the BQS at 1.5–4.5 h after warming (Figs. 1, 2 and 4). After 1.5 h of culture, the respiration activity of blastocysts in the hatched group was significantly higher than that of blastocysts in the degenerated group. An increase in the respiration rate as the preimplantation embryo develops to more advanced stages has been associated with an increase in energy demand for initiation of the compaction and blastocyst formation processes (Thompson *et al.*, 1996; Trimarchi *et al.*, 2000; Harvey *et al.*, 2002, 2004). Part of the

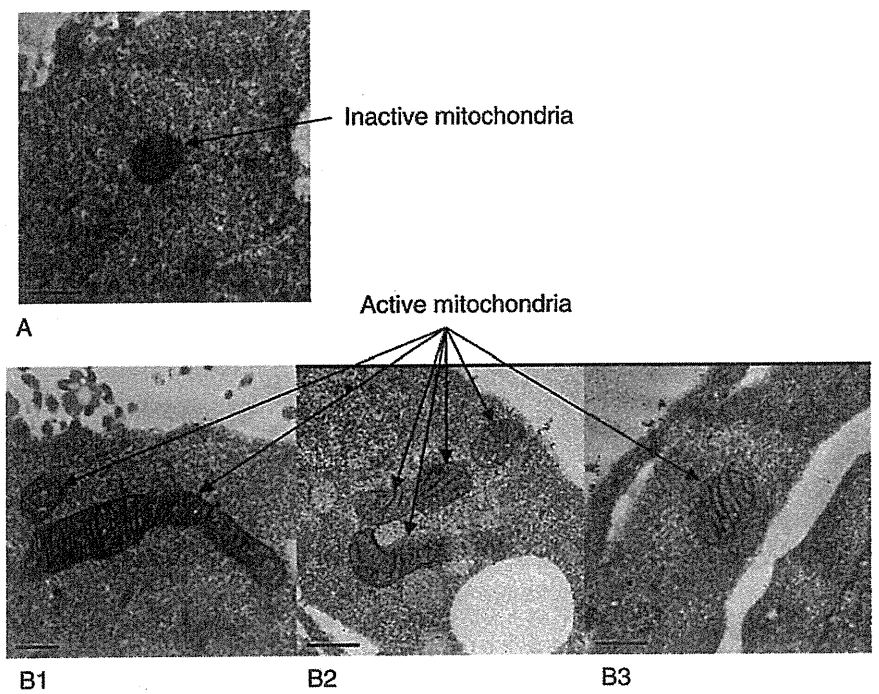

Figure 3 Observation of the CCO activity of mitochondria in blastocysts at 0 and 24 h after warming. DAB tetrahydrochloride is easily incorporated into mitochondria and oxidative polymerization occurs by high-voltage potential. Accordingly, mitochondria with CCO activity were stained as shown in (B1–B3). (**A**) Mitochondria in TE cell of blastocyst at 0 h after warming. (**B**) Mitochondria in TE cell (B1) and ICM (B2 and B3) of blastocyst at 24 h after warming. The CCO activity of mitochondria was detected in TE cells and ICM of blastocysts at 24 h, but not at 0 h. Bar = 0.5 μm.

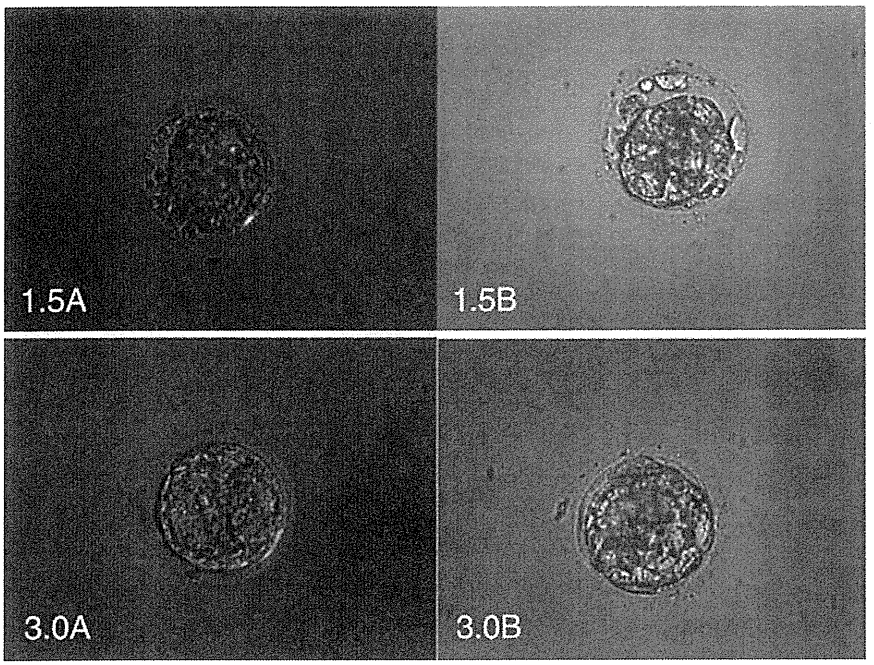

Figure 4 Morphologies of blastocysts at 1.5 and 3.0 h after warming. (**1.5A**) An embryo whose oxygen consumption was 4.1 fmol/s at 1.5 h and developed to a hatched blastocyst (hatched group). (**1.5B**) An embryo whose oxygen consumption at 1.5 h was 2.6 fmol/s and later degenerated (degenerated group). (**3.0A**) An embryo whose oxygen consumption was 6.3 fmol/s at 3 h and developed to a hatched blastocyst (hatched group). (**3.0B**) An embryo whose oxygen consumption at 3 h was 4.4 fmol/s and later degenerated. The embryos that went on to hatch and to degenerate had identical BQSs, 8 after 1.5 h and 12 after 3 h. Although there was no difference in morphology at 1.5–4.5 h after warming among groups, the oxygen consumption of embryos categorized in the hatched group was higher than that of degenerated at 1.5 h and than that of arrested and degenerated groups at 3.0–4.5 h.

ATP produced at the blastocyst level is the result of increased glycolysis and is therefore not related to oxygen consumption; nevertheless, 85% of the total ATP produced by the blastocyst is still generated by mitochondrial oxidative phosphorylation, a process that requires oxygen (Benos and Baladan, 1983; Leese, 2003). Thus, increased oxygen consumption corresponds approximately to ATP production. As a result, the developmental competence of blastocysts might be supported by prompt recovery of the respiratory ability.

In spite of blastocoel re-formation, the respiratory capacity of mitochondria of vitrified-warmed blastocysts was no >70% of that of non-vitrified blastocysts at 1.5 h after warming. Data obtained in this study suggest that the respiratory capacity of mitochondria recovers gradually with time and that the morphology of blastocysts immediately after warming does not correlate well with the oxygen consumption rate.

At 24 h after warming, a strong correlation was observed between oxygen consumption and cell number, which is consistent with the correlation observed in bovine embryos (Kaidi *et al.*, 2001; Lopes *et al.*, 2005). Therefore, selection based on morphology seems to be equal to oxygen consumption at this time. Thus, high-quality human blastocysts might be selected on the basis of the morphological criteria if vitrified-warmed blastocysts were cultured overnight after warming. However, in the clinical practice, the transfer of vitrified-warmed blastocysts is generally performed up to 5–6 h after warming. As shown in this study, there was no difference in blastocyst morphology degree until 4.5 h after thawing. On the other hand, the measurement of oxygen consumption might be used as a parameter to identify the embryo with better chances to develop further almost immediately after the warming procedure. This is because the blastocyst that developed to hatched stages at 24 h had the highest oxygen consumption levels by 1.5 h culture post-warming. In other words, a blastocyst with high potential could be selected almost immediately after warming based on the oxygen consumption rate, but not by using morphological assessment.

The results of the present study propose a new parameter for the selection of a single vitrified-warmed blastocyst for transfer that has high developmental potential. However, it must be taken into account that in this experimental set up, embryos could have been exposed to cellular stress since they have been periodically removed from the incubator for evaluation. Thus, an improvement of the technology should be put in place to measure oxygen consumption in more optimal conditions (i.e. inside an incubator atmosphere). In addition, further investigation including the relationship between blastocyst oxygen consumption and its developmental competence after transfer is required.

Authors' roles

M.Y., S.H., A.A. and Y.M. were equally involved in the literature review, experimental design, data acquisition, interpretation and analysis and manuscript preparation. T.I. and H.A. developed SCEM and were involved in data interpretation and analysis and manuscript preparation.

Acknowledgement

The authors thank Mr H. Matsumoto for his technical assistance.

Conflict of interest

T.I. works in a company producing SCEM. H.A. has shares in a company producing SCEM.

Funding

Part of this work was supported by a grant from the Japan Society for the Promotion of Science (JPS-RFTF 23580397 to S.H.).

References

Abe H, Shiku H, Aoyagi S, Hoshi H. In vitro culture and evaluation of embryos for production of high quality bovine embryos. *J Mamm Ova Res* 2004;**21**:22–30.

Andersen AN, Goossens V, Ferraretti AP, Bhattacharya S, Felberbaum R, de Mouzon J, Nygren KG. Assisted reproductive technology in Europe, 2004: results generated from European registers by ESHRE. *Hum Reprod* 2008;**23**:756–771.

Benos DJ, Baladan RS. Energy metabolism of preimplantation mammalian blastocysts. *Am J Physiol* 1983;**245**:40–45.

Donnay I, Leese HJ. Embryo metabolism during the expansion of the bovine blastocyst. *Mol Reprod Dev* 1999;**53**:171–178.

Gardner DK, Lane M. Culture and selection of viable human blastocysts: a feasible proposition for human IVF. *Hum Reprod Update* 1997; **3**:367–382.

Gopichandran N, Leese HJ. Metabolic characterization of the bovine blastocyst, inner cell mass, trophectoderm and blastocoel fluid. *Reproduction* 2003;**126**:299–308.

Harvey AJ, Kind KL, Thompson JG. REDOX regulation of early embryo development. *Reproduction* 2002;**123**:479–486.

Harvey AJ, Kind KL, Pantaleon M, Armstrong DT, Thompson JG. Oxygen-regulated gene expression in bovine blastocysts. *Biol Reprod* 2004;**71**:1108–1119.

Houghton FD. Energy metabolism of the inner cell mass and trophectoderm of the mouse blastocyst. *Differentiation* 2006;**74**:11–18.

Houghton FD, Thompson JG, Kennedy CJ, Leese HJ. Oxygen consumption and energy metabolism of the early mouse embryo. *Mol Reprod Dev* 1996;**44**:476–485.

Kaidi S, Bernard S, Lambert P, Massip A, Dessy F, Donnay I. Effect of conventional controlled-rate freezing and vitrification on morphology and metabolism of bovine blastocysts produced in vitro. *Biol Reprod* 2001;**65**:1127–1134.

Kuwayama M, Vajta G, Leda S, Kato O. Comparison of open and closed methods for vitrification of human embryos and the elimination of potential contamination. *Reprod Biomed Online* 2005; **11**:608–614.

Leese H. What does an embryo need? *Hum Fertil* 2003;**6**:180–185.

Lopes AS, Larsen LH, Ramsing NB, Løvendahl P, Räty M, Peippo J, Greve T, Callesen H. Respiration rates of individual bovine in vitro-produced embryos measured with a novel, non-invasive and highly sensitive microsensor system. *Reproduction* 2005;**130**:669–679.

Lopes AS, Madsen SE, Ramsing NB, Løvendahl P, Greve T, Callesen H. Investigation of respiration of individual bovine embryos produced in vivo and in vitro and correlation with viability following transfer. *Hum Reprod* 2007;**22**:558–566.

Magnusson C, Hillensjö T, Tsafriri A, Hurtborn R, Aheren K. Oxygen consumption of maturing rat oocytes. *Biol Reprod* 1977;**17**:9–15.

Magnusson C, Hillensjö T, Hamberger L, Nilsson L. Oxygen consumption by human oocytes and blastocysts grown in vitro. *Hum Reprod* 1986; **1**:183–184.

Mills RM, Brinster RL. Oxygen consumption of pre implantation mouse embryos. *Exp Cell Res* 1967;**47**:337–344.

Mohr LR, Trounson AO. Structural changes associated with freezing of bovine embryos. *Biol Reprod* 1981;**25**:1009–1025.

Nilsson B, Magnusson C, Widehn S, Hillensjo T. Correlation between blastocyst oxygen consumption and trophoblast cytochrome oxidase reaction at initiation of implantation of delayed mouse blastocysts. *J Embryol Exp Morphol* 1982;**71**:75–82.

Nonaka I, Koga Y, Ohtaki E, Yamamoto M. Tissue specificity in cytochrome c oxidase deficient myopathy. *J Neuro Sci* 1989;**92**:193–203.

Pandian Z, Templeton A, Serour G, Bhattacharya S. Number of embryos for transfer after IVF and ICSI: a Cochrane review. *Hum Reprod* 2005; **20**:2681–2687.

Rehman KS, Bukulmez O, Langley M, Carr BR, Nackley AC, Doody KM, Doody KJ. Late stages of embryo progression are a much better predictor of clinical pregnancy than early cleavage in intracytoplasmic sperm injection and in vitro fertilization cycles with blastocyst-stage transfer. *Fertil Steril* 2007;**87**:1041–1052.

Thompson JG, Partridge RJ, Houghton FD, Cox CI, Leese HJ. Oxygen uptake and carbohydrate metabolism by in vitro derived bovine embryos. *J Reprod Fertil* 1996;**106**:299–306.

Trimarchi JR, Liu L, Porterfield DM, Smith PJS, Keefe DL. Oxidative phosphorylation-dependent and -independent oxygen consumption by individual preimplantation mouse embryos. *Biol Reprod* 2000; **62**:1866–1874.

Utsunomiya T, Goto K, Nasu M, Kumasako Y, Araki Y, Yokoo M, Itoh-Sasaki T, Abe H. Evaluating the quality of human embryos with a measurement of oxygen consumption by scanning electrochemical microscopy. *J Mamm Ova Res* 2008;**25**:2–7.

Watson AJ. The cell biology of blastocyst development. *Mol Reprod Dev* 1992;**33**:492–504.

Wright VC, Chang J, Jeng G, Macaluso M. Assisted reproductive technology surveillance—United States, 2005. *MMWR Surveill Summ* 2008;**57**:1–23.

THE JOURNAL OF BIOLOGICAL CHEMISTRY VOL. 286, NO. 22, pp. 19682–19692, June 3, 2011
Printed in the U.S.A.

Secretoglobin 3A2 Suppresses Bleomycin-induced Pulmonary Fibrosis by Transforming Growth Factor β Signaling Down-regulation*[S]

Received for publication, March 10, 2011, and in revised form, April 8, 2011 Published, JBC Papers in Press, April 10, 2011, DOI 10.1074/jbc.M111.239046

Reiko Kurotani[‡§¶], Satoshi Okumura[§], Tsutomu Matsubara[‡], Utako Yokoyama[§], John R. Buckley[‡], Takeshi Tomita[‡], Kyohei Kezuka[§], Tomokazu Nagano[‡], Dominic Esposito[‖], Troy E. Taylor[‖], William K. Gillette[‖], Yoshihiro Ishikawa[§], Hiroyuki Abe[¶], Jerrold M. Ward[‡‡], and Shioko Kimura[‡1]**

From the [‡]Laboratory of Metabolism, NCI, National Institutes of Health, Bethesda, Maryland 20892, the [§]Cardiovascular Research Institute, Yokohama City University, Yokohama, Kanagawa, Japan 236-0004, [¶]Biochemical Engineering, Faculty of Engineering, Yamagata University, Yonezawa, Yamagata, Japan 992-8510, [‖]Protein Expression Laboratory, Advanced Technology Program, SAIC-Frederick, Inc. NCI, National Institutes of Health, Frederick, Maryland 21701, the [**]Cardiovascular Research Institute, Department of Cell Biology and Molecular Medicine and Medicine (Cardiology), New Jersey Medical School, University of Medicine and Dentistry of New Jersey, Newark, New Jersey 07103, and the [‡‡]Global VetPathology, Montgomery Village, Maryland 20866

With increasing worldwide rates of morbidity and mortality of pulmonary fibrosis, the development of effective therapeutics for this disease is of great interest. Secretoglobin (SCGB) 3A2, a novel cytokine-like molecule predominantly expressed in pulmonary airways epithelium, exhibits anti-inflammatory and growth factor activities. In the current study SCGB3A2 was found to inhibit TGFβ-induced differentiation of fibroblasts to myofibroblasts, a hallmark of the fibrogenic process, using pulmonary fibroblasts isolated from adult mice. This induction was through increased phosphorylation of STAT1 and expression of SMAD7 and decreased phosphorylation of SMAD2 and SMAD3. To demonstrate the effect of SCGB3A2 on the TGFβ signaling *in vivo*, a bleomycin-induced pulmonary fibrosis mouse model was used. Mice were administered bleomycin intratracheally followed by intravenous injection of recombinant SCGB3A2. Histological examination in conjunction with inflammatory cell counts in bronchoalveolar lavage fluids demonstrated that SCGB3A2 suppressed bleomycin-induced pulmonary fibrosis. Microarray analysis was carried out using RNAs from lungs of bleomycin-treated mice with or without SCGB3A2 and normal mice treated with SCGB3A2. The results demonstrated that SCGB3A2 affects TGFβ signaling and reduces the expression of genes involved in fibrosis. This study suggests the potential utility of SCGB3A2 for targeting TGFβ signaling in the treatment of pulmonary fibrosis.

An increasing number of people are affected by pulmonary fibrosis worldwide, with increasing morbidity and mortality rates. In the United States, the number of patients suffering from pulmonary fibrosis is about 200,000 (1, 2) (www.nhlbi.nih.gov). Recovery from pulmonary fibrosis is possible at early stages of the disease, whereas the recovery is limited once the fibrosis has progressed. A risk for developing pulmonary fibrosis increases by administration of bleomycin (BLM),[2] an anticancer and antibiotic agent, used in therapy for many types of solid tumors.

Fibrosis arises from inflammation initiated by cell injury, and injured tissues are gradually replaced by collagen fibers that are produced from fibroblasts and accumulate as myofibroblasts. Damaged cells produce chemokines, which stimulate leukocytes to proliferate and produce profibrotic cytokines such as transforming growth factor β (TGFβ), a major profibrotic growth factor, and interleukin-13 (IL-13), a major profibrotic mediator. TGFβ1 induces collagen type I transcription through the SMAD signaling, whereas IL-13 stimulates macrophages to produce TGFβ (3–6). On the other hand, interferon-γ (IFNγ) inhibits collagen generation through STAT1 activation followed by sequestration of p300, which plays a pivotal role in the regulation of collagen synthesis by TGFβ (7, 8). IFNγ also induces the antagonistic SMAD7, which in turn impairs TGFβ signaling through inhibition of the SMAD3 interaction with the TGFβ receptor (9) and/or disruption of formation of the TGFβ-induced functional SMAD-DNA complex (10). Other molecules are also involved in the fibrotic process (6). These include other Th2 cytokines such as IL-4, IL-5, and IL-10, chemokines such as CCL2 and CCL3, connective tissue growth factor, and platelet-derived growth factor (3, 11). Molecules involved in various pathways leading to myofibroblast expansion are considered to be useful as therapeutic targets. To this end, a number of inhibitors and/or monoclonal antibodies against these targeted molecules have been developed and subjected to clinical trials as a means to treat fibrosis (3, 11, 12). IFNγ is one of the targeted molecules used as a new therapy for

* This work was supported by the National Institutes of Health, Center for Cancer Research (Intramural Research Program of the NCI; NIH 0010190305 and Z01 BC010449-06, to S. K.). This work was also supported by Grant-in-aid for Young Scientists (B) (21790207, to R. K.).

[S] The on-line version of this article (available at http://www.jbc.org) contains supplemental Table S1 and S2 and Figs. S1–S5.

All effective genes were submitted to the Gene Expression Omnibus (GEO: ID GSE21560, www.ncbi.nlm.nih.gov).

[1] To whom correspondence should be addressed: Bldg. 37, Rm. 3106, NIH, Bethesda, MD 20892. Tel.: 301-496-0958; Fax: 301-496-8419; E-mail: kimuras@mail.nih.gov.

[2] The abbreviations used are: BLM, bleomycin; SCGB, secretoglobin; CHX, cycloheximide; GO, gene ontology; MMPs, metalloproteinases; qRT, quantitative RT; BALF, bronchoalveolar lavage fluid; αSMA, α smooth muscle actin; rm, recombinant mouse.

fibrosis (5, 6, 12); however, because of potentially harmful side effects, a better alternative is desirable (13).

Secretoglobin (SCGB) 3A2, previously called uteroglobin-related protein 1, is a member of the SCGB gene superfamily (14). The SCGB gene superfamily consists of 3 gene families; family 1 has 4 subfamilies, each composed of 3–11 members, family 2 consists of 2 subfamilies, each with 6–10 members, and family 3 consists of only one subfamily with 5 members (15, 16). All members of the SCGB gene superfamily are cytokine-like secreted proteins of ~10 kDa, found only in mammals. They form homodimers or heterodimers with other members. Most functions of SCGB are still elusive, and the signaling pathways including a possible receptor(s) that transmits activities of these proteins is not known. Among the best studied member of the gene superfamily is SCGB1A1, also called uteroglobin, Clara cell secretory protein, or Clara cell 10-kDa protein that exhibits anti-inflammatory and immunomodulatory activities in lung (17–19). Studies on the mechanisms of the anti-inflammatory activity of SCGB1A1 have been carried out (20, 21). Other members such as SCGB2A2 (mammaglobin A) and SCGB1D2 (lipophilin B) are known as a cancer marker for mammary gland (22) (23).

SCGB3A2 is the second member of the SCGB family 3, subfamily A. It is predominantly expressed in lung airways. SCGB3A2 was found to play a role in suppression of lung inflammation using a mouse model for allergic airway inflammation (24) and to promote branching and maturation of mouse fetal lungs (25). MARCO (macrophage scavenger receptor with collagenous structure), expressed in alveolar macrophages in lung, was suggested as a possible receptor for SCGB3A2 (26). On the other hand, we have demonstrated the possible presence of a SCGB3A2-specific receptor on the mesenchymal cells of mouse fetal lungs (25). Despite these studies, very little is known about the biological and physiological functions of SCGB3A2 and its mechanisms of action including the receptor and the signaling pathway it provokes.

In the present study SCGB3A2 was found to inhibit the TGFβ signaling through increased STAT1 phosphorylation and expression of SMAD7 and decreased phosphorylation of SMAD2/3, thus resulting in inhibition of TGFβ-induced myofibroblast differentiation. In an *in vivo* mouse model, SCGB3A2 markedly suppressed BLM-induced pulmonary fibrosis, suggesting the potential use of SCGB3A2 as a novel therapeutic reagent to treat pulmonary fibrosis.

EXPERIMENTAL PROCEDURES

Isolation and Primary Culture of Lung Fibroblasts—Lung tissues from 7–9-week-old female mice were cut into small pieces, mounted on collagen type I-coated 60-mm plate (IWAKI, Shizuoka, Japan), and then cultured for 7 days. Fibroblasts were harvested by 0.5% trypsin and 0.53 mM EDTA in PBS, washed with DMEM supplemented with 10% FBS, plated on a 35-mm plate, and cultured for 16 h. Fibroblasts were stimulated by 10 ng/ml TGFβ (Sigma) in DMEM containing 3% FBS for 24–72 h in the presence or absence of recombinant mouse (rm) SCGB3A2 (2.5 μg/ml). The recombinant mouse SCGB3A2 (rmSCGB3A2) was purified as described (25) (detailed purification method of SCGB3A2 will be provided upon request). For simplicity "SCGB3A2" is used instead of rmSCGB3A2 throughout the manuscript. For blocking experiments of IFNγ receptor signaling, a specific antibody against IFNγ receptor (rat anti-CD119 clone GR20, BD, Tokyo, Japan) was co-cultured with SCGB3A2 or IFNγ (R & D Systems, Minneapolis, MN) for 24 h or 30 min, respectively. To determine translational regulatory mechanism, fibroblasts were incubated with SCGB3A2 (2.5 μg/ml) and cycloheximide (CHX, 1 μg/ml, WAKO, Osaka, Japan) for 3 h or pretreated with CHX 3 h before stimulation with IFNγ. To down-regulate Stat1 expression, Stat1 siRNA probes (no. 7 probe, sense strand (5′-GCAUCUUACUGAAGGUGAATT-3′) and antisense strand (5′-UUCACCUUCAGUAAGAUGCAT-3′) and no. 8 probe (sense strand 5′-GAGUUGGUUUAAUAUAUAUTT-3′) and antisense strand (5′-AUAUAUAUUAAACCAACUCAT-3′); Qiagen, Valencia, CA) were transfected into fibroblasts using Lipofectamine 2000 (Invitrogen) 48 h before addition of TGFβ and/or SCGB3A2.

Immunoblotting—Immunoblotting was performed using the following antibodies; anti-STAT1, anti-pSTAT1 (Tyr-701), anti-SMAD2, anti-pSMAD2 (Ser-465/467), anti-SMAD3 (Cell Signaling Technology, Danvers, MA), anti-pSMAD3 (Ser-423/425) (Millipore Corp. Temecula, CA), anti-SMAD7 (Santa Cruz Biotechnology, Inc. Santa Cruz, CA), anti-α-smooth muscle actin (αSMA; Sigma), and anti-β-actin (Sigma). Immunoblotting was performed as described in Kurotani *et al.* (25). All immunoreactive bands were visualized using ECL (GE Healthcare) or ImmunoStar LD (WAKO) with LAS-3000mini (FUJIFILM, Tokyo, Japan) and then standardized by immunoreactive band of β-actin using Multi Gauge Version 3.0 software (FUJIFILM).

Quantitative RT-PCR and RT-PCR—Total RNAs isolated using TRIzol (Invitrogen) and digested with DNase I were reverse-transcribed by Superscript II reverse transcriptase (Invitrogen). Quantitative RT-PCR (qRT-PCR) was performed with ABI Prism 7900 Sequence Detection System (Applied Biosystems, Foster City, CA) using SYBR Green master mixture. The standard curve method was used, and all data were normalized to 18 S rRNA amplified using TaqMan Ribosomal RNA Control Reagent, VIC Probe (Applied Biosystems). RT-PCR was performed using AmpliTaq Gold DNA polymerase (Applied Biosystems) with iCycler (Bio-Rad). PCR condition used was 50 °C for 2 min and 95 °C for 10 min followed by 95 °C for 15 s and 60 °C for 40 s for 40 cycles. Primers used for qRT-PCR and RT-PCR analysis are summarized in supplemental Table S1. Leukocytes isolated from normal mouse spleen were stimulated by phorbol 12-myristate 13-acetate, (10 ng/ml) (Calbiochem) and ionomycin (1 μM) (Calbiochem) for 3 h or by poly(I:C) (polyinosinic-polycytidylic acid potassium salt, 10 μg/ml; Imgenex, San Diego, CA) for 24 h. The mRNAs extracted were used as a positive control for IFNγ and IFNα (27) and for IFNβ, respectively (28).

Animals and SCGB3A2 Treatment—C57BL/6N mice (NCI-Frederick, National Institutes of Health) were maintained under a standard 12-h light/12-h dark cycle with water and chow provided *ad libitum*. At least ten 7–8-week-old C57BL/6N mice were prepared for each group. Eight units/kg BLM (Sigma) or PBS was directly administered once by intratracheal intubation into C57BL/6N mice using the BioLITE sys-

tem (BioTex, Inc., Houston, TX). Purified SCGB3A2 (1.5 mg/kg/day) or PBS was intravenously administered to mice via the tail vein once daily for a week starting on day 14 after BLM administration. Four groups of mice were used in this study; administration of BLM followed by intravenous injection of PBS (Group 1) or SCGB3A2 (Group 2) or administration of PBS followed by intravenous injection of PBS (Group 3) or SCGB3A2 (Group 4). All animal studies were performed after approval by the National Cancer Institute Animal Care and Use Committee. SCGB3A2 used in the animal study contained endotoxin at 0.2 enzyme units/mg. The dose of SCGB3A2 was determined based on the previous study in which a total of 200 μg, but not 100 μg, exhibited growth factor activity without causing any gross abnormalities to the dam as well as the embryos (25). For microarray analysis, C57BL/6N mice (7–8 weeks old) were treated with PBS or SCGB3A2 by intravenous administration and were euthanized 12 h later.

Bronchoalveolar Lavage—On day 21 after administration of BLM, mice were euthanized and subjected to bronchoalveolar lavage. Bronchoalveolar lavage fluid (BALF) was obtained by intratracheal instillation of 1 ml of PBS into the lung while it was kept in the thoracic cavity. Cells in the BALF were centrifuged at 500 × *g* and subjected to Diff-Quick (Baxter Healthcare, Miami, FL) staining. Cells were identified and counted using 2000–2500 cells from 10 fields randomly chosen. Tissues were fixed in 4% paraformaldehyde or stored at −80 °C for later RNA preparation.

Pathology—The whole lung was inflated and fixed with 4% paraformaldehyde. Lung tissues were embedded in paraffin, and 4-μm whole lung sections were prepared. Hematoxylin and eosin staining was carried out for assessment of BLM-induced fibrosis. Masson's Trichrome staining (Sigma) was used to detect collagen fibers. Immunohistochemical staining for SCGB3A2, pSMAD2, pSMAD3, and SMAD2/3 was performed in BLM-treated lungs using anti-mouse SCGB3A2 antibody (produced in our laboratory) (14), anti-pSMAD2(ser465/467) (Cell Signaling Technology), anti-pSMAD3 (Epitomics, Burlingame, CA), and anti-SMAD2/3 (BD Biosciences), respectively. For antigen-retrieval, the sections were incubated in Tris-EDTA (pH 6.0) at a temperature over 95 °C for 10 min before protein blocking. The immunoreactivities were enhanced by ABC method (Vector Laboratories, Burlingame, CA) followed by visualization using diaminobenzidine (DakoCytomation, Carpinteria, CA) and counterstained with hematoxylin. Immunocytochemical staining for αSMA was performed as described (29, 30). Briefly, fibroblasts cultured on 8-well Lab Tek Chamber Glass Slide (Nalge Nunc International, Naperville, IL) with and without TGFβ and/or SCGB3A2 were incubated at room temperature in PBS containing 0.1% Triton X 100 for 15 min followed by fixing with 4% paraformaldehyde for 15 min at room temperature. Cells were incubated with anti-αSMA antibody (Sigma, 1:400) overnight at 4 °C after blocking with 3% BSA-PBS for 1 h at room temperature. Cells were incubated with Alexa Fluor 488 goat anti-mouse IgG (Invitrogen) for 30 min at room temperature in dark. Nuclei were stained by 1 mg/ml DAPI (4′,6-diamino-2-phenylindole) (47). The αSMA signal was observed using Nikon EC (Nikon, Tokyo, Japan).

Fibrosis Assessment (Grading)—The grade of BLM-induced pulmonary fibrosis was determined based on the percentage of the fibrotic area in the whole lung section as follows; the presence of fibrosis in 0–25% of the lung for Grade 1, 26–50% of the lung for Grade 2, 51–75% of the lung for Grade 3, and 76–100% of the lung for Grade 4. No fibrosis, but with inflammation including a few infiltrating foci of lymphocytes or a very small granulomas, was considered Grade 0.

DNA Microarray—Total RNAs were purified using TRIzol and RNAeasy (Qiagen, Valencia, CA) from lungs of four groups (Group 1, 2, 3, and 4) of mice as described above or mice 12 h after SCGB3A2 treatment. Ten (group mice analysis) or 20 μg (SCGB3A2 treatment) of purified total RNA were reverse-transcribed to label with Cy3 and Cy5 (GE Healthcare) using the FairPlay Microarray Labeling kit (Stratagene, La Jolla, CA) or SuperScript™ Indirect cDNA Labeling Core kit (Invitrogen), respectively. Microarray analysis was carried out using individually isolated RNA from at least 5 mice in each group and mouse array chips (45K) obtained from the NCI Microarray Facility. Experiments and analysis were performed according to the manufacturer's instruction and the instruction of the Center for Cancer Research, NCI (nciarray.nci.nih.gov). Gene Ontology (GO) analysis (31) and pathway analysis were performed using a mouse gene data (Mm-Std_20060628.gdb) and a mouse pathway data (Mm_Contributed_20070917) from MAPPFinder (32). Up-regulated genes were sorted based on scores (ratio of Cy5 per Cy3) more than 2.0 (average) between Group 1 and Group 3, more than 1.5 (average) between Group1 and Group2, and those up-regulated in all reactions.

Statistical Analysis—Data are shown as the mean ± S.D. from indicated numbers of independent experiments. Statistical analysis was performed one-way ANOVA followed by Bonferroni multiple comparison test.

RESULTS

Effect of SCGB3A2 on Differentiation of Fibroblasts into Myofibroblasts—It was previously demonstrated that SCGB3A2 has at least two biological functions; an anti-inflammatory function was revealed using an ovalbumin-induced allergic airway inflammation model (24), and growth factor activity was studied using *ex vivo* fetal lung organ cultures and *in vivo* injection of SCGB3A2 to pregnant mice (25). To obtain insight into whether SCGB3A2 plays any additional roles in lung physiology and/or diseases, primary fibroblasts obtained from adult mouse lungs were used as an *in vitro* model of fibrosis in which the effect of SCGB3A2 on TGFβ-induced differentiation of fibroblasts into myofibroblasts was studied (33). Inhibition of this transformation would indicate a role for SCGB3A2 in controlling fibrosis. As expected, TGFβ treatment resulted in differentiation of pulmonary fibroblasts to myofibroblasts within 24 h as clearly seen by the characteristic myofibroblast morphology and the robust expression of αSMA (Fig. 1*A*, *TGFβ*, αSMA is seen in *green*). In contrast, treatment of fibroblasts with both TGFβ and SCGB3A2 together (TGFβ+SCGB3A2) exhibited morphology and the level of αSMA expression similar to those of normal fibroblasts (Fig. 1*A*, *Cont. versus TGFβ+SCGB3A2*). SCGB3A2 alone did not have any effect on the morphology of fibroblasts (Fig. 1*A*, *SCGB3A2*). Note that the number of cells

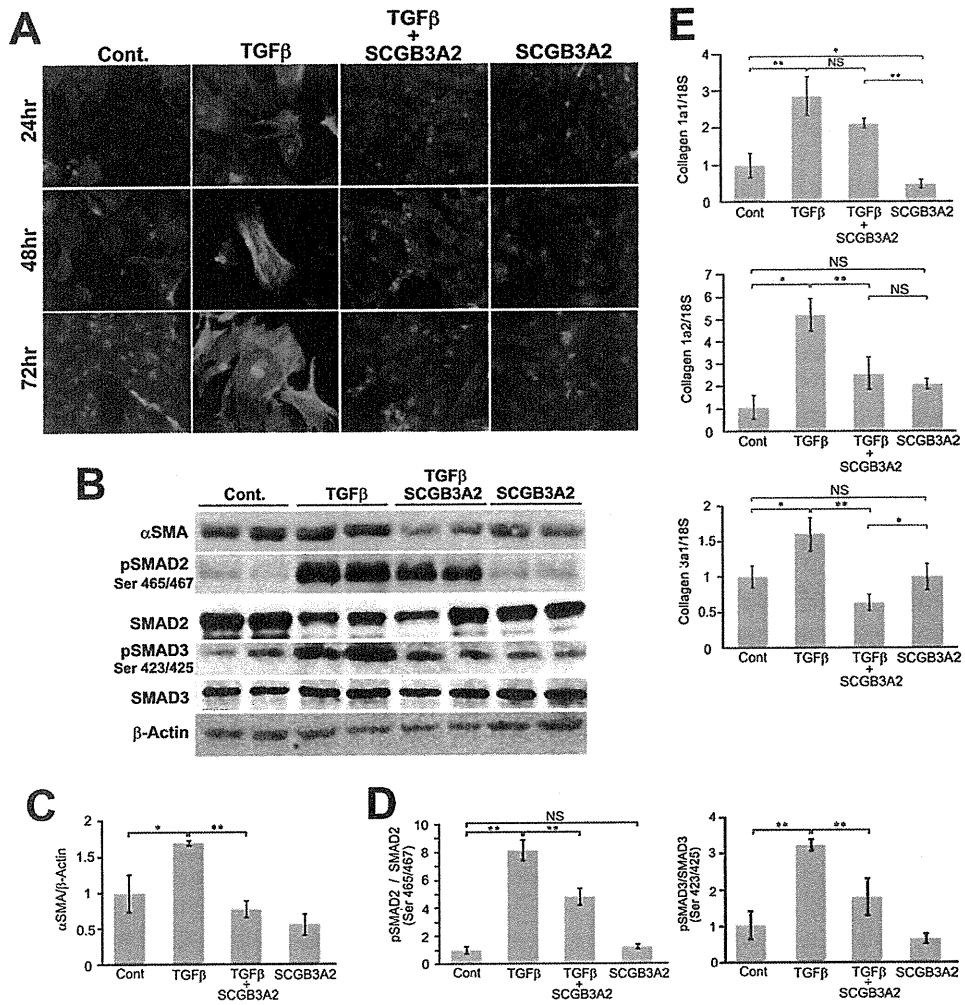

FIGURE 1. **Inhibition of differentiation from fibroblast to myofibroblast by SCGB3A2.** *A*, representative immunocytochemistry for αSMA ($n = 4$) is shown. αSMA was visualized as a *green signal*. Fibroblasts isolated from adult mouse lungs were cultured in the absence (*Cont.*; normal fibroblast) or the presence of SCGB3A2, TGFβ, or TGFβ and SCGB3A2 together for 24–72 h. All the images were taken at ×600 (original magnification). *B*, representative immunoblotting results for αSMA, phosphorylated SMAD2 (*pSMAD2*), total SMAD2, phosphorylated SMAD3 (*pSMAD3*), total SMAD3, and β-actin using cells harvested after 24 h stimulation are shown. *C*, and *D*, densitometric analysis of the immunoblot signals in *B* is shown as the mean ± S.D. ($n = 4$) for αSMA (*C*) and pSMAD2/SMAD2 and pSMAD3/SMAD3 ratios (*D*). *E*, qRT-PCR for collagen 1a1, collagen 1a2, and collagen 3a1 is shown. Fibroblasts were harvested 24 h after stimulation and were subjected to qRT-PCR analysis to determine the level of collagen genes expression. *Cont*, normal fibroblast as control; *TGFβ*, stimulated by TGFβ; *TGFβ+SCGB3A2*, administration of both TGFβ and SCGB3A2; *SCGB3A2*, fibroblast stimulated by SCGB3A2 only. The graph shows the mean ± S.D. from 4–8 lungs per group, each in triplicate. *, $p < 0.05$; **, $p < 0.01$; *NS*, not significant.

did not significantly differ among different culture groups for at least up to 72 h (data not shown). The level of αSMA protein was increased by TGFβ treatment, which returned to control levels in cells treated with SCGB3A2 as determined by Western blotting performed after 24 h of stimulation with TGFβ (Fig. 1, *B* and *C*). SCGB3A2 alone did not have a significant effect on the level of αSMA protein as compared with control. When SMAD2 and SMAD3, the major molecules in the TGFβ signaling pathway, were examined, phosphorylated SMAD2 (*pSMAD2*) and SMAD3 (*pSMAD3*) were increased by TGFβ treatment as expected, and combined treatment with TGFβ and SCGB3A2 partially reversed the increase (Fig. 1, *B* and *D*). Again, SCGB3A2 alone did not have any effect on SMAD2 and SMAD3 phosphorylation. Furthermore, qRT-PCR analysis revealed that the expression of collagen 1a2 and collagen 3a1 was decreased in fibroblasts stimulated by TGFβ and SCGB3A2 together as compared with those treated with TGFβ alone (Fig. 1*E*). Because production of a complete collagen fiber requires three collagens (34), the reduced expression of two collagen genes is likely to account for the reduced Type I and Type III collagen fibers. The effect of SCGB3A2 on the reduced expression of collagen genes was abolished when SCGB3A2 was boiled before the addition to the media, suggesting that the effect of SCGB3A2 was not due to any contaminants in SCGB3A2 preparation (supplemental Fig. S1). These results demonstrated that SCGB3A2 inhibited TGFβ-induced differentiation of primary lung fibroblasts to myofibroblasts.

Induction of STAT1 Phosphorylation and SMAD7 Expression by SCGB3A2—Immunoblotting was performed to examine levels of SMAD7 protein and the status of STAT1 phosphorylation in the presence or absence of TGFβ and/or SCGB3A2 (Fig. 2). It is well documented that IFNγ treatment results in phosphorylation of STAT1 and induces SMAD7 expression, which interferes with the TGFβ signaling (9, 35). In mouse lung primary fibroblasts, the expression of SMAD7, STAT1, and phosphorylated STAT1 was hardly detectable in control and TGFβ-

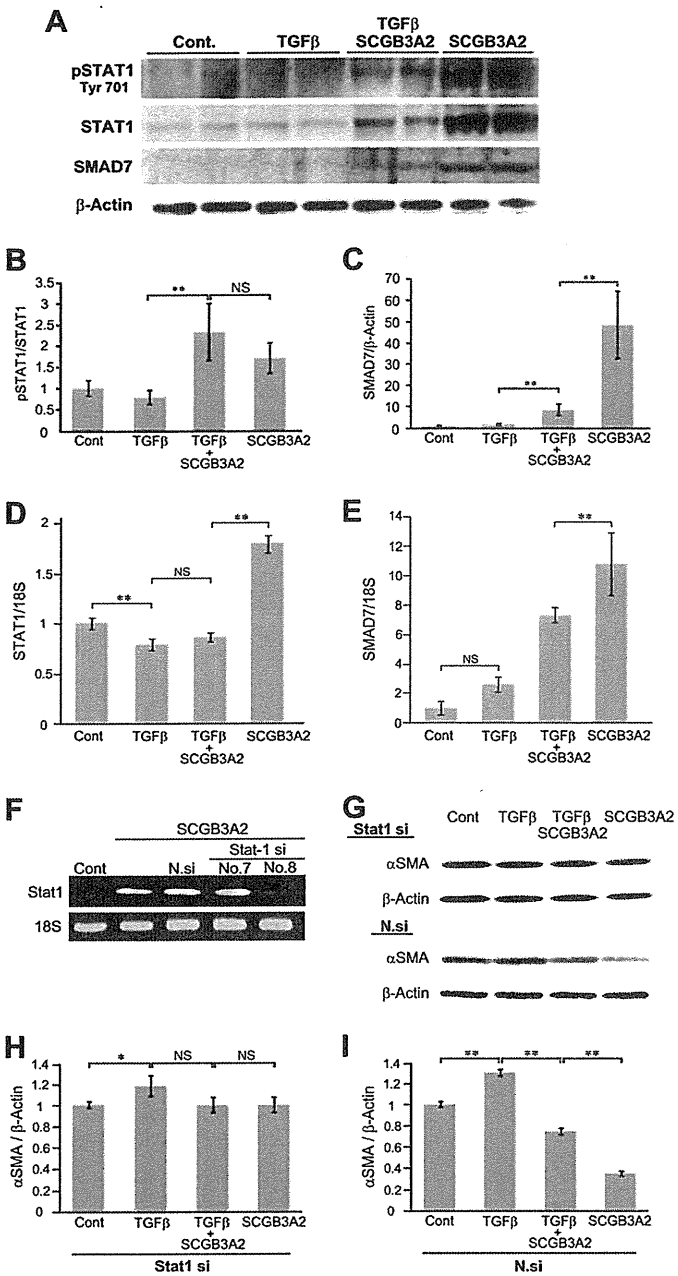

FIGURE 2. **Phosphorylation of STAT1 and SMAD7 expression by SCGB3A2.** *A*, immunoblotting for phosphorylated STAT1 (*pSTAT1*), total STAT1, SMAD7, and β-actin as control is shown. *B* and *C*, shown is a graph for densitometric analysis of the immunoblot signals shown in *A* for pSTAT1/STAT1 (*B*) and SMAD7/β-actin (*C*). The mean ± S.D. ($n = 4$) is shown. *D* and *E*, qRT-PCR for STAT1 (*D*) and SMAD7 (*E*) using 18 S as an internal control is shown. *NS*, not significant. *F–I*, effect of STAT1 siRNA or nonspecific control siRNA on the level of αSMA is shown. *F*, qRT-PCR to confirm knockdown of STAT1 mRNA with STAT1 siRNA probes is shown. *G*, immunoblotting for αSMA and β-actin using cells transfected with no. 8-STAT1 siRNA probe (*STAT1 si*) or nonspecific negative siRNA probe (*N.si*). *H* and *I*, shown is a graph for densitometric analysis of the immunoblot signals shown in *G* for αSMA/β-actin with a STAT1 siRNA probe (*H*) and nonspecific negative siRNA probe (*I*). The mean ± S.D. ($n = 4$) is shown. Fibroblasts were harvested 24 h after stimulation. *Cont*, normal fibroblast as control; *TGFβ*, stimulated by TGFβ; *TGFβ+SCGB3A2*, administration of both TGFβ and SCGB3A2; *SCGB3A2*, fibroblast stimulated by SCGB3A2 only. **, $p < 0.01$, *NS*, not significant. Representative immunoblotting results are shown.

treated cells (Fig. 2*A*). In contrast, the level of STAT1, phosphorylated STAT1 (pSTAT1), and SMAD7 was markedly increased when fibroblasts were treated with SCGB3A2 (Fig. 2, *A–C*). TGFβ dramatically inhibited the induction of STAT1 and SMAD7 by SCGB3A2 (see *TGFβ+SCGB3A2 versus SCGB3A2*), whereas the pSTAT1/STAT1 ratio stayed at similar levels with TGFβ+SCGB3A2 and SCGB3A2-only treatments (Fig. 2*B*). The SCGB3A2-induced increase of STAT1 and SMAD7 expression was due to an mRNA increase as demonstrated by qRT-PCR (Fig. 2, *D* and *E*, respectively). When STAT1 siRNA was transfected to mouse lung primary fibroblasts followed by treatment with TGFβ and/or SCGB3A2, TGFβ-induced αSMA expression levels stayed the same with and without SCGB3A2 (Fig. 2, *G* and *H*). With control nonspecific negative siRNA, TGFβ-induced αSMA expression was reduced by SCGB3A2 as expected (Fig. 2*I*), confirming that the effect of SCGB3A2 is through STAT1. These data demonstrated that SCGB3A2 enhanced expression of SMAD7 and STAT1 and phosphorylation of STAT1, resulting in inhibition of the TGFβ signaling pathway.

Relationship between SCGB3A2 and Interferon γ Receptor—Several cytokines are known to activate STAT1. Among them, the key cytokine that activates STAT1 is IFNγ (36). IFNγ is known to improve fibrosis through phosphorylation of STAT1 (5, 6, 12), and its clinical effect on pulmonary fibrosis is well documented (37). IFNα and IFNβ also activate STAT1 and inhibit fibrosis (38–40). RT-PCR analysis using lung primary fibroblasts demonstrated that IFNγ was not expressed in lung primary fibroblasts regardless of SCGB3A2 treatment (Fig. 3*A*). Similarly, neither IFNα nor IFNβ was expressed in lung primary fibroblasts stimulated by SCGB3A2 (supplemental Fig. S2). In the following studies, we focused on the relationship between SCGB3A2 and IFNγ and its receptor. When IFNγ receptor-specific neutralizing antibody was added to the culture, IFNγ-induced phosphorylation of STAT1 was inhibited, whereas it did not inhibit phosphorylation of STAT1 induced by SCGB3A2 (Fig. 3*B*). Interestingly, it took ~3 h for the SCGB3A2-induced phosphorylation of STAT1 to reach maximum levels (Fig. 3*C*). This was unusually long as compared with the IFNγ-induced STAT1 phosphorylation, which reached maximal levels within 30 min of stimulation (41, 42) (supplemental Fig. S3). Furthermore, SCGB3A2-stimulated STAT1 phosphorylation was suppressed in the presence of CHX (Fig. 3*D*). In contrast, IFNγ-stimulated STAT1 phosphorylation was unchanged with and without CHX treatment (Fig. 3*E*). These data indicated that SCGB3A2 promoted phosphorylation of STAT1 in a manner independent of IFNγ receptor and through a CHX-sensitive intermediate molecule. These data further suggested that the SCGB3A2-STAT1 signaling may have been through a SCGB3A2-specific receptor.

Inhibition of BLM-induced Lung Fibrosis by SCGB3A2—To validate these *in vitro* data that SCGB3A2 suppresses the TGFβ signaling pathway resulting in reduction of fibrosis, mice were subjected to a pulmonary fibrosis model. Pulmonary fibrosis was induced by direct administration of BLM or PBS as control to mice by intratracheal intubation. The histopathology of the lungs on day 14 (2 weeks) after BLM treatment did not reveal any fibrosis regardless of treatment regimens (data not shown). At day 14, mice received the first of 7 daily consecutive intravenous injections of SCGB3A2 or PBS through the tail vein (Fig. 4*A*). On day 21 after BLM administration, pulmonary fibrosis

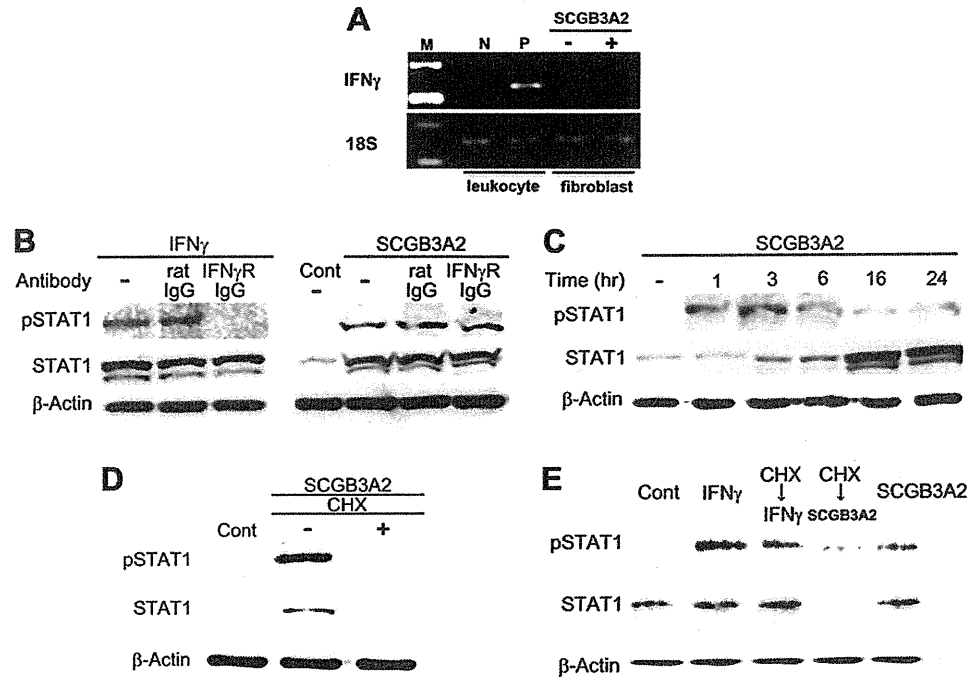

FIGURE 3. **Relationship between SCGB3A2 and IFNγ receptor.** *A*, representative RT-PCR for IFNγ in fibroblasts in the presence or absence of SCGB3A2 (n = 3) is shown. Leukocytes stimulated by phorbol 12-myristate 13-acetate (10 ng/ml) and ionomycin (1 μM) for 3 h were used as a positive control for IFNγ. *B*, shown are blocking experiments for IFNγ receptor signaling. A representative result is shown (n = 3). pSTAT1 was detected in the presence of anti-IFNγ receptor antibody and SCGB3A2 (*right panel*). *C*, a representative time-course result of STAT1 phosphorylation by SCGB3A2 (n = 3) is shown. *D* and *E*, protein synthesis blocking experiments are shown. Fibroblasts were incubated with both SCGB3A2 and CHX (1 μg/ml) for 3 h (*D* and *E* for CHX→SCGB3A2) or were preincubated with CHX (1 μg/ml) for 3 h before stimulation with IFNγ for 15 min (*E*). A representative result is shown (n = 3).

was observed in the lungs of BLM-treated group of mice (Group 1). The extent of fibrosis was rated as grade 1 to grade 2 (Fig. 4*B*). In contrast, mice in Group 2 that received BLM and SCGB3A2 did not develop any pulmonary fibrosis except one mouse of five tested. In Group 3, one mouse exhibited small fibrotic lesions, whereas no fibrosis was observed in Group 4 mice. Collagen fibers were found to focally occupy the alveolar space of mice in Group 1 but not in other groups of lungs as determined by Masson's Trichrome staining, which detects collagen fibers (Fig. 4*C*, *upper panel*). Excessive SCGB3A2 expression was focally found in a part of airway epithelial cells and the foci of fibrosis of Group 1 mouse lungs (Fig. 4*C*, *lower panel*). In contrast, other groups of lungs (Groups 2–4) expressed SCGB3A2 at similar levels in airway epithelial cells as expected, although Group 2 lungs appeared to have slightly higher expression than Group 3 and 4 lungs. When the expression of total SAMD2/3 as well as pSMAD2 and pSMAD3 was examined by immunohistochemistry, all were highly up-regulated in most of airway epithelial cells as well as the foci of fibrosis in Group 1 mouse lungs, whereas expression stayed at similar levels and patterns in other groups of lungs including those of BLM+SCGB3A2 administered mouse lungs (Group 2) (supplemental Fig. S4). The latter results suggested that SCGB3A2 appeared to have suppressed expression of SMAD2/3 and/or pSMAD2 and pSMAD3 in epithelial as well as parenchymal cells. The numbers of macrophages and neutrophils in BALF were enhanced by BLM treatment, whereas they were markedly reduced to levels close to that of controls in the SCGB3A2-treated group (Fig. 4*D*). The number of lymphocytes was not different with statistical significance among the four groups (data not shown). These data indicated that development of BLM-induced fibrosis was suppressed by the daily administration of SCGB3A2 on the third week of BLM treatment.

Alteration of Gene Expression by BLM and/or SCGB3A2—To determine the genes whose expression was altered in the BLM-induced lung fibrosis and/or SCGB3A2-induced reduction of fibrosis, microarray analysis was carried out using mRNAs obtained from lungs of mice between Group 1 (BLM-treated) and Group 3 (PBS control) and Group 1 (BLM-treated) and Group 2 (BLM- and SCGB3A2-treated). With a cutoff of >1.5-fold change in expression, 1646 and 1275 genes were, respectively, up- and down-regulated by BLM as compared with control PBS (between Group 1 and Group 3), and 346 and 919 genes were, respectively, up- and down-regulated by SCGB3A2 treatment as compared with no SCGB3A2 treatment in BLM treated mice (between Group 1 and Group 2). Using these genes, GO (gene ontology) analysis was performed for the changes caused by BLM and for the effect of SCGB3A2 in BLM-treated mice (heat map results are shown in supplemental Fig. S5). The results revealed that "Inflammatory response" and "Response to wounding" under "Biological Process" and "Extracellular region part," "Extracellular region," and "Extracellular space" under "Cellular Component" were overexpressed by BLM injury (Table 1) and suppressed by administration of SCGB3A2 (Table 2). Additionally, to demonstrate genes that are altered by SCGB3A2, microarray analysis was carried out using lung RNAs of normal mice that were intravenously administered SCGB3A2 and were euthanized 12 h later. GO analysis revealed that "Signal transducer activity" and "Molec-

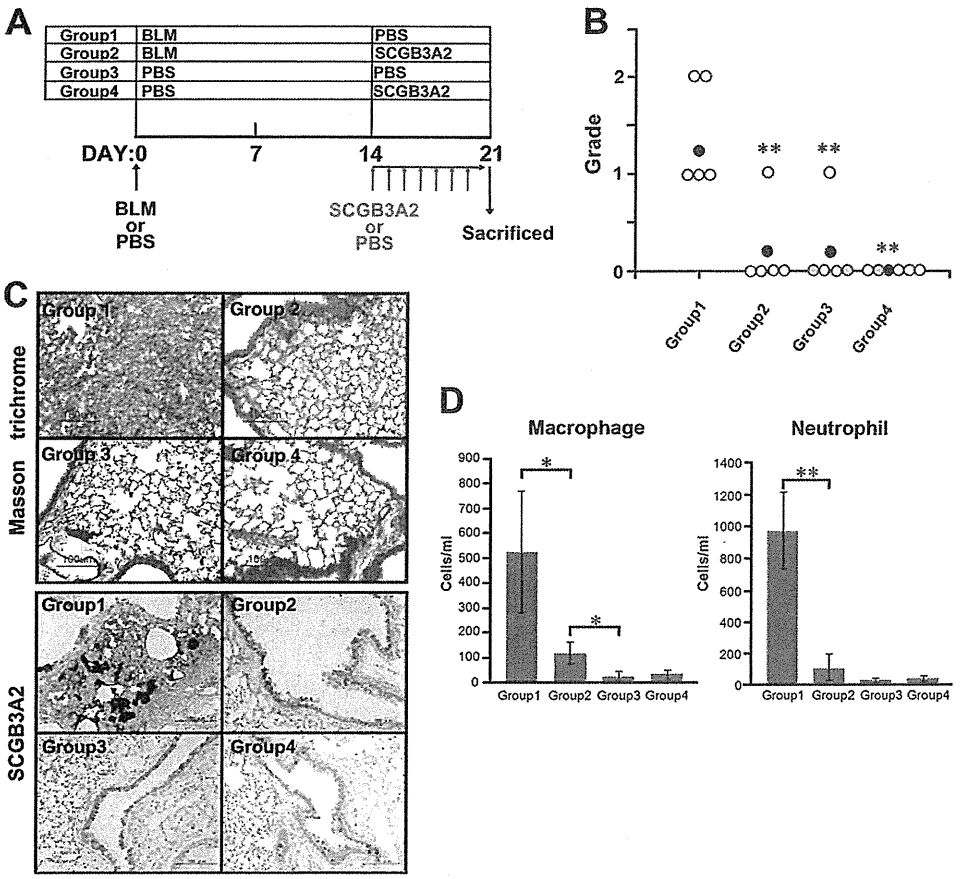

FIGURE 4. **Inhibition of BLM-induced lung fibrosis by SCGB3A2.** *A*, shown is a scheme to prepare BLM-induced fibrosis model mice. BLM or PBS was administered to the lungs of C57BL/6N mice by intratracheal intubation at day 0. SCGB3A2 or PBS was administered to mice by intravenous injection once daily for a week starting at day 14 followed by euthanasia at day 21. The four groups of mice were subjected to the studies as shown. PBS was administered as a control in Groups 3 and 4. Whole experiments were carried out at least twice. *B*, grading of fibrosis carried out as described under "Experimental Procedures." BLM administration resulted in production of fibrous tissue, focally or diffusely in lungs of Group 1, whereas no fibrous tissue formation was observed in four of five lungs exposed to BLM followed by SCGB3A2 treatment in Group 2. *White circle*, no lesions; *black circle*, mean ($n = 5$); *gray*, presence of a few infiltrating foci of lymphocytes or very small granulomas. **, $p < 0.01$, Group 1 *versus* Groups 2, 3, or 4. *C*, Masson's Trichrome staining and immunohistochemistry for SCGB3A2 are shown. Collagen fibers were focally detected as a blue color by Masson trichrome staining in the parenchyma of the lungs of mice in Group 1 but not the lungs of other groups. Excessive SCGB3A2 expression was found in a part of the epithelial cells and in the foci of fibrosis as a brown color by immunohistochemistry in Group 1. Representative staining is shown ($n = 5$). *D*, shown are the number of macrophages and neutrophils in BALF. The number of macrophages and neutrophils increased by BLM (*Group 1*) was significantly decreased by administration of SCGB3A2 (*Group 2*), especially neutrophils which reduced to the levels of control (*Group 3* and *Group 4*). The graph shows the mean ± S.D. from 5 lungs per group ($n = 5$). *, $p < 0.05$; **, $p < 0.01$.

ular transducer activity" categorized by only one term "Molecular Function" were up-regulated by short-term treatment of SCGB3A2 (Table 3). The TGFβ signaling was among the top pathways identified by the Pathway Mapping program (Fig. 5), further supporting our conclusion that SCGB3A2 affects the TGFβ signaling pathway.

Further analysis revealed that the expression of matrix metalloproteinases (MMPs) and other extracellular matrix (ECM)-degrading enzymes that degrade damaged tissues as well as enzymes synthesizing collagen I, fibronectin, hyaluronic acid, and other components of wound provisional ECM was altered after BLM and/or SCGB3A2 treatment (supplemental Table S2). qRT-PCR was performed to confirm the alterations of gene expression in BLM-treated lungs with (Group 2) and without (Group 1) SCGB3A2 (Fig. 6). High levels of MMP2, MMP12, and MMP14 expression in BLM-treated lungs (Group 1) were significantly decreased by the administration of SCGB3A2 (Group 2); in particular, MMP14 returned to the levels of the "no BLM treatment" groups (Group 3 and 4). Cathepsin S and D that belong to a group of proteinases were also highly expressed in BLM-treated group (Group 1), and decreased to a level similar to control by SCGB3A2 (Group 2). Cathepsin C levels did not show any statistically significant difference among the four groups of mice. These data further indicated a role for SCGB3A2 in suppression of lung fibrosis induced by BLM.

DISCUSSION

This study revealed that SCGB3A2 possesses anti-fibrotic activity as revealed by *in vitro* cell culture studies with primary lung fibroblasts and *in vivo* studies using a BLM-induced pulmonary fibrosis model mouse. SCGB3A2, a member of the SCGB gene superfamily composed of secretory proteins of small molecular weight, is predominantly expressed in lung airways (14, 43). The most studied member of the SCGB gene superfamily, namely SCGB1A1, also called uteroglobin, Clara cell 10-kDa protein, or Clara cell secretory protein, is a multifunctional protein with anti-inflammatory/immunomodulatory properties with manifestation of antichemotactic, antiallergic, antitumorigenic, and embryonic growth-stimulatory activities (19). The current study revealed that the related pro-

TABLE 1
GO terms for overexpressed genes in BLM-injured lung

Gene ontology term	Cluster frequency[a]	Total frequency[b]	Corrected *p* value[c]
	%	%	
Biological Process, cell adhesion	6.40	3.50	2.92×10^{-5}
Biological adhesion	6.40	3.50	2.92×10^{-5}
Antigen processing and presentation of exogenous peptide antigen	0.70	0.10	0.00654
Immune system process	6.30	3.90	0.01711
Inflammatory response	2.70	1.30	0.01977
Antigen processing and presentation of peptide antigen via MHC class II	0.60	0.10	0.02221
Antigen processing and presentation of exogenous peptide antigen via MHC class II	0.60	0.10	0.02221
Antigen processing and presentation of peptide of polysaccharide antigen via MHC class II	0.60	0.10	0.04108
Response to wounding	3.30	1.80	0.04663
Cellular Component			
Extracellular region part	18.00	12.70	5.62×10^{-7}
Extracellular matrix	4.00	1.70	1.05×10^{-6}
Proteinaceous extracellular matrix	3.39	1.70	1.68×10^{-6}
Extracellular region	20.40	15.10	5.57×10^{-6}
Extracellular space	16.80	12.00	7.62×10^{-6}
Molecular function			
Carbohydrate binding	3.00	1.60	0.04087

[a] Frequency of Entrez Gene IDs appeared in a given GO term based on those having over 0.585 in log ratio.
[b] Frequency of Entrez Gene IDs appeared in a given GO term based on all genes.
[c] *p* value corrected using the Bonferroni method.

TABLE 2
GO terms for suppressed genes by SCGB3A2 in BLM-injured lung

Gene ontology term	Cluster frequency[a]	Total frequency[b]	Corrected *p* value[c]
	%	%	
Biological process			
Defense response	6.10	2.50	6.78×10^{-5}
Response to external stimulus	6.40	2.70	7.91×10^{-5}
Response to wounding	4.50	1.80	0.00172
Response to stimulus	15.80	10.60	0.00896
Inflammatory response	3.20	1.30	0.03692
Cellular component			
Extracellular region	24.50	15.10	1.82×10^{-9}
Extracellular region part	20.40	12.70	2.26×10^{-7}
Extracellular space	19.50	12.00	3.22×10^{-7}

[a] Frequency of Entrez Gene IDs appeared in a given GO term based on those having over 0.585 in log ratio.
[b] Frequency of Entrez Gene IDs appeared in a given GO term based on all genes.
[c] *p* value corrected using the Bonferroni method.

TABLE 3
GO terms overexpressed by SCGB3A2 in normal lung

Gene ontology term, molecular function	Cluster frequency[a]	Total frequency[b]	Corrected *p* value[c]
	%	%	
Signal transducer activity	20.7	15.9	0.0378
Molecular transducer activity	20.7	15.9	0.0378

[a] Frequency of Entrez Gene IDs appeared in a given GO term based on those having over 0.585 in log ratio.
[b] Frequency of Entrez Gene IDs appeared in a given GO term based on all genes.
[c] *p* value corrected using the Bonferroni method.

tein SCGB3A2 at therapeutic levels has novel biological activity toward induced fibrosis in addition to its known anti-inflammatory (24) and growth factor activities (25). SCGB1A1 was previously suggested to be a novel cytokine (44). The current results support the notion that the SCGB gene superfamily may be a novel cytokine family. The anti-inflammatory, growth factor and anti-fibrotic activities that SCGB3A2 possesses may suggest a potential use for this protein in the treatment of many lung diseases, including lung fibrosis as demonstrated in this study.

BLM administered by intratracheal intubation induced pulmonary fibrosis, which focally occupied the pulmonary parenchyma by 3 weeks after BLM administration. Interestingly, BLM-induced fibrosis was almost completely suppressed by SCGB3A2 treatment, which interfered with the infiltration of neutrophils and macrophages into lung and the expression of fibrosis related-genes such as collagens, fibronectin, elastin, cathepsins, and MMPs, all of which were up-regulated by BLM. The development of fibrosis was hardly detectable by the end of 2 weeks after BLM administration, suggesting that SCGB3A2 might inhibit development of fibrosis when given at its early stages.

The anti-fibrotic activity of SCGB3A2 appears to be exerted through STAT1 phosphorylation, induction of SMAD7, and inhibition of SMAD2/3 phosphorylation, which results in suppression of the TGFβ signaling, ultimately leading to the inhibition of myofibroblasts formation. Interestingly, this is the exact pathway that IFNγ exhibits its anti-fibrotic activity (9, 35). We initially hypothesized that SCGB3A2 may induce the expression of IFNγ, thereby suppressing TGFβ signaling. However, the SCGB3A2 pathway is likely to be distinct from the IFNγ pathway based on the following reasons; 1) IFNγ-induced phosphorylation of STAT1 and increased expression of SMAD7 usually occurs within 10–30 min after IFNγ stimulation (supplemental Fig. S3) (9, 41, 42, 45), whereas it took ~3 h for SCGB3A2 to induce maximum levels of STAT1 phosphorylation, 2) SCGB3A2 did not induce IFNγ mRNA expression as determined by RT-PCR, 3) IFNγ receptor neutralizing antibody (46) did not block SCGB3A2-induced STAT1 phosphorylation, and 4) CHX ablated the expression of pSTAT1 in fibroblasts treated with SCGB3A2 but not IFNγ. These results suggest the involvement of a newly synthesized protein upon SCGB3A2 stimulation other than IFNγ in the SCGB3A2-pSTAT1 pathway. In this regard it is interesting to note that STAT1 was induced by SCGB3A2 in a CHX-sensitive fashion. SMAD7 was also induced by SCGB3A2. The SCGB3A2-induced increase of STAT1 and SMAD7 expression was dramatically inhibited by TGFβ at the mRNA levels. However the pSTAT1/STAT1 ratio stayed the same. The involvement of STAT1 in the SCGB3A2 pathway was confirmed by STAT1 siRNA experiments, in which no decrease of αSMA was observed in

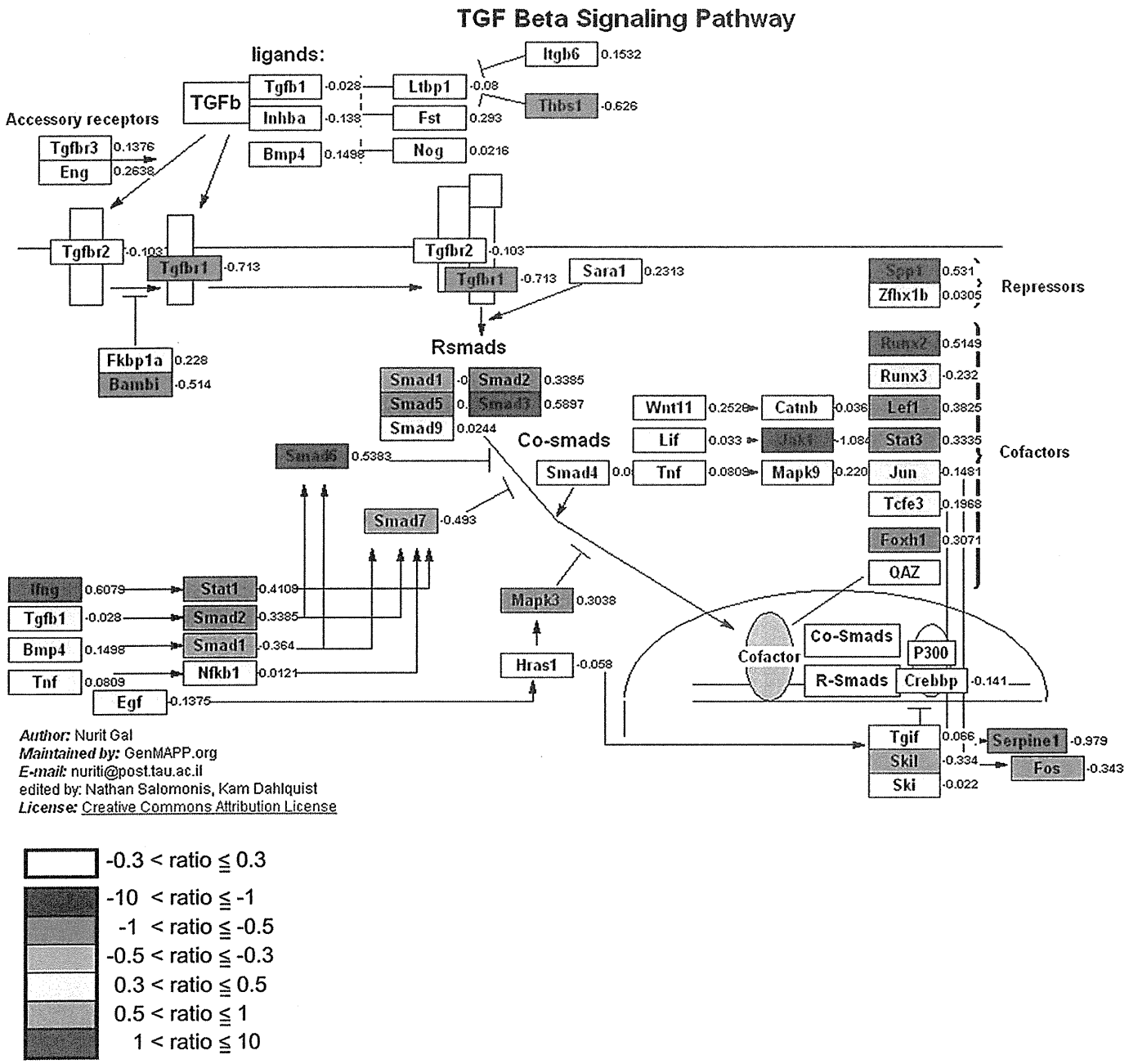

FIGURE 5. **Effect of SCGB3A2 on TGFβ signaling pathway.** Pathway analysis of microarray data showed that the TGFβ signaling pathway was affected by administration of SCGB3A2. Median -fold differences from seven separate samples for each gene on which microarray analysis were run are color-coded based on the *scale* shown at the *bottom left*.

TGFβ+SCGB3A2-treated cells as compared with TGFβ only treatment. These results together suggest that the SCGB3A2-pSTAT1-SMAD7 signaling pathway may be through a SCGB3A2-specific receptor that is distinct from the IFNγ receptor (Fig. 7). We previously suggested the presence of a SCGB3A2-specific receptor-like molecule on the surface of pulmonary mesenchymal cells (25). The nature of the CHX-sensitive intermediate molecule(s), a SCGB3A2-specific receptor, and the mechanism(s) for the inhibitory effect of TGFβ on the induction of STAT1 and SMAD7 by SCGB3A2 are currently not known. Further experiments are required to address these questions. Other cytokines/molecules such as IFNα, IFNβ, epidermal growth factor, growth hormone, and estrogen are known to activate STAT1 (47). Among them, neither IFNα nor IFNβ was induced by SCGB3A2 in mouse lung primary fibroblasts, suggesting that they are not likely involved in the SCGB3A2-pSTAT1-SMAD7 pathway. The involvement of the other cytokines/molecules in the SCGB3A2-pSTAT1 pathway needs to be examined.

Inflammation is the first to occur after BLM administration followed by fibrosis (3–6). In animal models the fibrosis stage starts ~1 week after BLM administration (3). In our BLM model, SCGB3A2 was administered at the fibrosis period and exhibited anti-fibrotic activity through blocking the TGFβ signaling pathway. We previously demonstrated using mice-exogenously administered SCGB3A2 that SCGB3A2

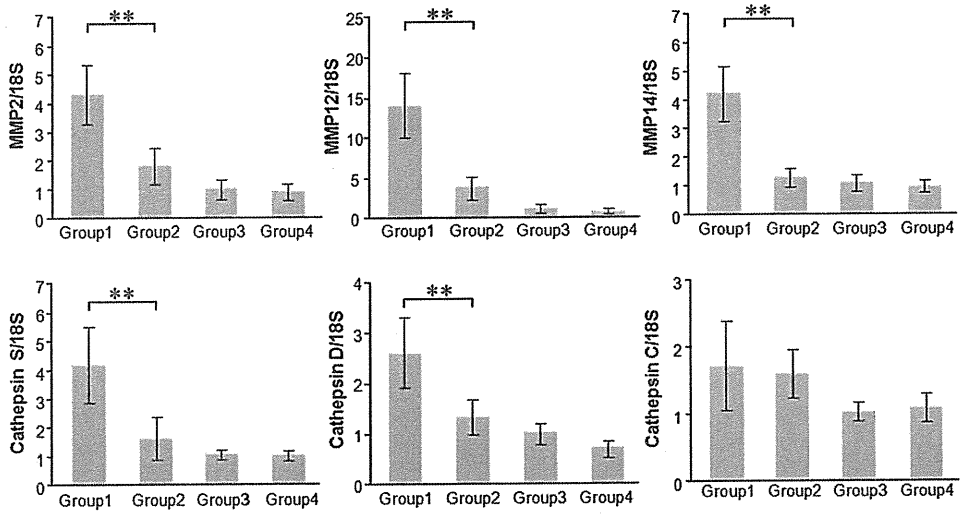

FIGURE 6. **Confirmation of microarray data by qRT-PCR.** Expression levels of MMP2, MMP12, MMP14, cathespin S, cathespin D, and cathespin C mRNAs relative to 18 S were determined by qRT-PCR using mRNAs prepared from mouse lungs of Groups 1–4 as described in Fig. 4. The *graph* shows the mean ± S.D. from 4–9 lungs per group, each in triplicate. **, $p < 0.01$.

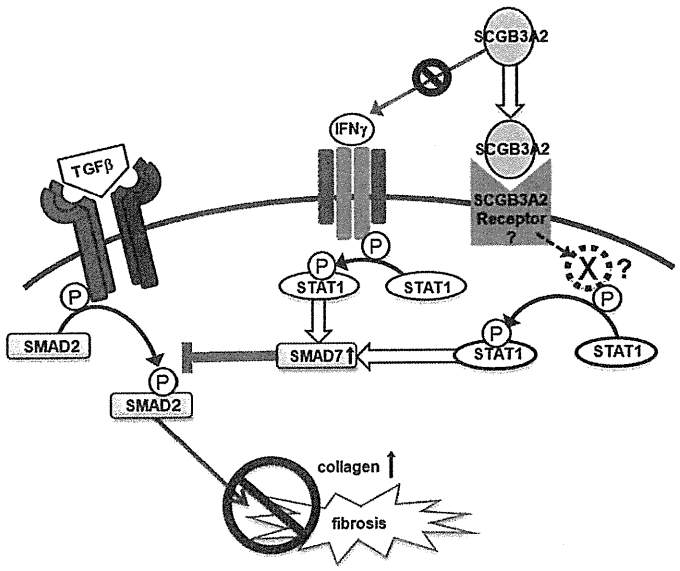

FIGURE 7. **Schematic diagram for the SCGB3A2-induced inhibition of the TGFβ signaling pathway.** SCGB3A2 inhibits collagen production through STAT1 phosphorylation and increases expression of SMAD7, which inhibits TGFβ-mediated SMAD2/3 activation. A newly synthesized molecule *X* mediates the SCGB3A2-induced STAT1 phosphorylation.

exhibits anti-inflammatory activities. We do not know whether SCGB3A2, if administered at the beginning of BLM administration, exerts anti-inflammatory activities and reduces the damage otherwise caused by BLM. Furthermore, we do not know whether endogenous SCGB3A2 regulates pulmonary inflammation and/or fibrosis. However, the following evidence suggests a role for SCGB3A2 in inflammation in lung *in vivo*; in the ovalbumin-induced allergic airway inflammation model mouse, SCGB3A2 expression is reduced in the airways (24, 48, 49), and the plasma SCGB3A2 levels are significantly lower in severe asthmatics without oral corticosteroid treatment as compared with mild- or moderate-asthma patients and controls (50). In the current study, a rather strong focal SCGB3A2 expression was found in a part of epithelial cells, and overexpressed SCGB3A2 was accumulated in fibrotic foci of lungs of mice subjected to BLM. However, it should be noted that these lungs are already at late stages, having developed BLM-induced fibrosis. In BLM+SCGB3A2-treated lungs, SCGB3A2 expression is in similar patterns but is slightly up-regulated to those found in control mice. Whether SCGB3A2 is down-regulated right after BLM administration needs to be determined.

Although IFNγ has been used as a therapy for pulmonary fibrosis (5, 6, 12), it causes a number of potentially harmful side effects and thus is not useful for advanced fibrosis (nlm.nih.gov (13)). In this study SCGB3A2 signaling was found to cross-talk with the IFNγ except at the beginning of the pathway. This suggests that SCGB3A2 could be potentially useful in treating fibrosis, in particular pulmonary fibrosis. More importantly, SCGB3A2 can be administered intratracheally. SCGB3A2 is almost exclusively expressed in lung (14) and is present at relatively high levels in the BALF of normal lungs (24). Thus, delivering a protein into a place where the protein is naturally present in high amounts would probably not cause toxicities. Alternatively, SCGB3A2 can be administered intravenously. Indeed, SCGB3A2 growth factor activity was previously demonstrated *in vivo* by intravenous administration of SCGB3A2 to pregnant female mice through the tail vein resulting in advanced development of fetal lungs (25). In that study, no gross abnormalities were observed in any fetal organs after intravenous SCGB3A2 administration. Furthermore, histological examination of the dam's lung did not show any abnormalities. Based on these facts, it is likely that SCGB3A2 may potentially improve pulmonary fibrosis without harmful side effects as seen with IFNγ. It is possible that BLM treatment as a chemotherapy reagent may not damage the lung if SCGB3A2 is given at the same time. However, additional studies are necessary to determine the efficacy of SCGB3A2 in treating pulmonary fibrosis in humans.

In conclusion, the present study demonstrated that SCGB3A2 inhibits TGFβ signaling through increased STAT1 phosphorylation and expression of SMAD7 and decreased phosphorylation of SMAD2/3, leading to inhibition of myofi-

broblast differentiation. The inhibitory effect of SCGB3A2 on myofibroblast differentiation was reproduced using a BLM-induced lung fibrosis model mouse, in which the severity of lung fibrosis was reduced by SCGB3A2 administration.

Acknowledgments—We thank Drs. Lalage Wakefield, Kathleen Flanders, and Frank Gonzalez (NCI, National Institutes of Health) for advice and critical review of the manuscript and Michie Kobayashi for microarray analysis (DNA Chip Research Inc., Yokohama, Japan).

REFERENCES

1. Coultas, D. B., Zumwalt, R. E., Black, W. C., and Sobonya, R. E. (1994) *Am. J. Resp. Crit. Care Med.* **150,** 967–972
2. Crystal, R. G., Bitterman, P. B., Mossman, B., Schwarz, M. I., Sheppard, D., Almasy, L., Chapman, H. A., Friedman, S. L., King, T. E., Jr., Leinwand, L. A., Liotta, L., Martin, G. R., Schwartz, D. A., Schultz, G. S., Wagner, C. R., and Musson, R. A. (2002) *Am. J. Respir. Crit. Care Med.* **166,** 236–246
3. Moeller, A., Ask, K., Warburton, D., Gauldie, J., and Kolb, M. (2008) *Int. J. Biochem. Cell Biol.* **40,** 362–382
4. Cutroneo, K. R., White, S. L., Phan, S. H., and Ehrlich, H. P. (2007) *J. Cell. Physiol.* **211,** 585–589
5. Tzortzaki, E. G., Antoniou, K. M., Zervou, M. I., Lambiri, I., Koutsopoulos, A., Tzanakis, N., Plataki, M., Maltezakis, G., Bouros, D., and Siafakas, N. M. (2007) *Respir. Med.* **101,** 1821–1829
6. Wynn, T. A. (2004) *Nat. Rev. Immunol.* **4,** 583–594
7. Eickelberg, O., Pansky, A., Koehler, E., Bihl, M., Tamm, M., Hildebrand, P., Perruchoud, A. P., Kashgarian, M., and Roth, M. (2001) *FASEB J.* **15,** 797–806
8. Ghosh, A. K., and Varga, J. (2007) *J. Cell. Physiol.* **213,** 663–671
9. Ulloa, L., Doody, J., and Massagué, J. (1999) *Nature* **397,** 710–713
10. Zhang, S., Fei, T., Zhang, L., Zhang, R., Chen, F., Ning, Y., Han, Y., Feng, X. H., Meng, A., and Chen, Y. G. (2007) *Mol. Cell Biol.* **27,** 4488–4499
11. Scotton, C. J., and Chambers, R. C. (2007) *Chest* **132,** 1311–1321
12. Puente, N. A., Aliotta, J. M., and Passero, M. A. (2007) *Med. Health R. I.* **90,** 43–45
13. Selman, M. (2003) *Am. J. Respir. Crit. Care Med.* **167,** 945–946
14. Niimi, T., Keck-Waggoner, C. L., Popescu, N. C., Zhou, Y., Levitt, R. C., and Kimura, S. (2001) *Mol. Endocrinol.* **15,** 2021–2036
15. Reynolds, S. D., Reynolds, P. R., Pryhuber, G. S., Finder, J. D., and Stripp, B. R. (2002) *Am. J. Respir. Crit. Care Med.* **166,** 1498–1509
16. Klug, J., Beier, H. M., Bernard, A., Chilton, B. S., Fleming, T. P., Lehrer, R. I., Miele, L., Pattabiraman, N., and Singh, G. (2000) *Ann. N.Y. Acad. Sci.* **923,** 348–354
17. Shijubo, N., Kawabata, I., Sato, N., and Itoh, Y. (2003) *Curr. Pharm. Des.* **9,** 1139–1149
18. Wang, S. Z., Rosenberger, C. L., Bao, Y. X., Stark, J. M., and Harrod, K. S. (2003) *J. Immunol.* **171,** 1051–1060
19. Mukherjee, A. B., Zhang, Z., and Chilton, B. S. (2007) *Endocr. Rev.* **28,** 707–725
20. Mandal, A. K., Zhang, Z., Ray, R., Choi, M. S., Chowdhury, B., Pattabiraman, N., and Mukherjee, A. B. (2004) *J. Exp. Med.* **199,** 1317–1330
21. Miele, L. (2000) *Ann. N.Y. Acad. Sci.* **923,** 128–140
22. Watson, M. A., and Fleming, T. P. (1996) *Cancer Res.* **56,** 860–865
23. Culleton, J., O'Brien, N., Ryan, B. M., Hill, A. D., McDermott, E., O'Higgins, N., and Duffy, M. J. (2007) *Int. J. Cancer* **120,** 1087–1092
24. Chiba, Y., Kurotani, R., Kusakabe, T., Miura, T., Link, B. W., Misawa, M., and Kimura, S. (2006) *Am. J. Respir. Crit. Care Med.* **173,** 958–964
25. Kurotani, R., Tomita, T., Yang, Q., Carlson, B. A., Chen, C., and Kimura, S. (2008) *Am. J. Respir. Crit. Care Med.* **178,** 389–398
26. Bin, L. H., Nielson, L. D., Liu, X., Mason, R. J., and Shu, H. B. (2003) *J. Immunol.* **171,** 924–930
27. Maeng, H. G., Lim, H., Jeong, Y. J., Woo, A., Kang, J. S., Lee, W. J., and Hwang, Y. I. (2009) *Immunobiology* **214,** 311–320
28. Lin, Y. C., Huang, D. Y., Chu, C. L., and Lin, W. W. (2010) *Mol. Immunol.* **47,** 1569–1578
29. Asazuma-Nakamura, Y., Dai, P., Harada, Y., Jiang, Y., Hamaoka, K., and Takamatsu, T. (2009) *Exp. Cell Res.* **315,** 1190–1199
30. Kurotani, R., Yoshimura, S., Iwasaki, Y., Inoue, K., Teramoto, A., and Osamura, R. Y. (2002) *J. Endocrinol.* **172,** 477–487
31. Ashburner, M., Ball, C. A., Blake, J. A., Botstein, D., Butler, H., Cherry, J. M., Davis, A. P., Dolinski, K., Dwight, S. S., Eppig, J. T., Harris, M. A., Hill, D. P., Issel-Tarver, L., Kasarskis, A., Lewis, S., Matese, J. C., Richardson, J. E., Ringwald, M., Rubin, G. M., and Sherlock, G. (2000) *Nat. Genet.* **25,** 25–29
32. Doniger, S. W., Salomonis, N., Dahlquist, K. D., Vranizan, K., Lawlor, S. C., and Conklin, B. R. (2003) *Genome Biol.* **4,** R7
33. Tomasek, J. J., Gabbiani, G., Hinz, B., Chaponnier, C., and Brown, R. A. (2002) *Nat. Rev. Mol. Cell Biol.* **3,** 349–363
34. Shoulders, M. D., and Raines, R. T. (2009) *Annu. Rev. Biochem.* **78,** 929–958
35. Weng, H., Mertens, P. R., Gressner, A. M., and Dooley, S. (2007) *J. Hepatol.* **46,** 295–303
36. Yu, H., Pardoll, D., and Jove, R. (2009) *Nat. Rev. Cancer* **9,** 798–809
37. Luppi, F., Losi, M., D'Amico, R., Fabbri, L. M., and Richeldi, L. (2009) *Sarcoidosis Vasc. Diffuse Lung Dis.* **26,** 64–68
38. Azuma, A., Li, Y. J., Abe, S., Usuki, J., Matsuda, K., Henmi, S., Miyauchi, Y., Ueda, K., Izawa, A., Sone, S., Hashimoto, S., and Kudoh, S. (2005) *Am. J. Respir. Cell Mol. Biol.* **32,** 93–98
39. Senft, A. P., Taylor, R. H., Lei, W., Campbell, S. A., Tipper, J. L., Martinez, M. J., Witt, T. L., Clay, C. C., and Harrod, K. S. (2010) *Am. J. Respir. Cell Mol. Biol.* **42,** 404–414
40. Papatheodoridis, G. V., Petraki, K., Cholongitas, E., Kanta, E., Ketikoglou, I., and Manesis, E. K. (2005) *J. Viral. Hepat.* **12,** 199–206
41. Tamai, M., Kawakami, A., Tanaka, F., Miyashita, T., Nakamura, H., Iwanaga, N., Izumi, Y., Arima, K., Aratake, K., Huang, M., Kamachi, M., Ida, H., Origuchi, T., and Eguchi, K. (2006) *J. Lab. Clin. Med.* **147,** 182–190
42. Seo, J. Y., Kim, D. Y., Lee, Y. S., and Ro, J. Y. (2009) *Cytokine* **46,** 51–60
43. Tomita, T., Kido, T., Kurotani, R., Iemura, S., Sterneck, E., Natsume, T., Vinson, C., and Kimura, S. (2008) *J. Biol. Chem.* **283,** 25617–25627
44. Mukherjee, A. B., Kundu, G. C., Mantile-Selvaggi, G., Yuan, C. J., Mandal, A. K., Chattopadhyay, S., Zheng, F., Pattabiraman, N., and Zhang, Z. (1999) *Cell. Mol. Life Sci.* **55,** 771–787
45. Lee, Y. J., and Benveniste, E. N. (1996) *J. Immunol.* **157,** 1559–1568
46. Cheng, M., Nguyen, M. H., Fantuzzi, G., and Koh, T. J. (2008) *Am. J. Physiol. Cell Physiol.* **294,** C1183–C1191
47. Krämer, O. H., and Heinzel, T. (2010) *Mol. Cell Endocrinol.* **315,** 40–48
48. Chiba, Y., Kusakabe, T., and Kimura, S. (2004) *Am. J. Physiol. Lung Cell Mol. Physiol.* **287,** L1193–L1198
49. Chiba, Y., Srisodsai, A., Supavilai, P., and Kimura, S. (2005) *Immunol. Lett.* **97,** 123–129
50. Inoue, K., Wang, X., Saito, J., Tanino, Y., Ishida, T., Iwaki, D., Fujita, T., Kimura, S., and Munakata, M. (2008) *Allergol. Int.* **57,** 57–64

ZOOLOGICAL SCIENCE 28: 790–801 (2011)

A Novel Deletion Mutation of Mouse Ruby-eye 2 Named *ru2^{d}/Hps5$^{ru2\text{-}d}$* Inhibits Melanocyte Differentiation and Its Impaired Differentiation is Rescued by L-tyrosine

Tomohisa Hirobe[1,2*], Chihiro Yoshihara[3], Sakae Takeuchi[3], Kazumasa Wakamatsu[4], Shosuke Ito[4], Hiroyuki Abe[5], Yoko Kawa[6] and Yoshinao Soma[6]

[1]*Radiation Effect Mechanisms Research Group, National Institute of Radiological Sciences, Chiba 263-8555, Japan*
[2]*Graduate School of Science, Chiba University, Chiba 263-8522, Japan*
[3]*Graduate School of Science and Technology, Okayama University, Okayama, Japan*
[4]*Department of Chemistry, Fujita Health University School of Health Sciences, Toyoake, Japan*
[5]*Graduate School of Science and Technology, Yamagata University, Yonezawa, Japan*
[6]*Department of Dermatology, St. Marianna University School of Medicine, Kawasaki, Japan*

In our laboratory, a single autosomal recessive mutation in a phenotype similar to ruby-eye (*ru/Hps6^{ru}*) or ruby-eye 2 (*ru2/Hps5^{ru2}*) spontaneously occurred in siblings of C57BL/10JHir (+/+, black) mice in 2006. RT-PCR analysis revealed that this novel mutation, named *ru2^{d}/Hps5$^{ru2\text{-}d}$*, exhibited frameshift by 997G deletion in the *Hps5* gene. To clarify the mechanism of the hypopigmentation, the characteristics of proliferation and differentiation of *ru2^{d}/ru2^{d}* epidermal melanoblasts and melanocytes cultured in a serum-free medium were investigated. The proliferation of *ru2^{d}/ru2^{d}* melanoblasts and melanocytes did not differ from that of +/+ melanoblasts and melanocytes. However, the differentiation of *ru2^{d}/ru2^{d}* melanocytes was greatly inhibited. Tyrosinase (TYR) activity, expression of TYR, TYR-related protein 1 (TRP1) and TRP2 (dopachrome tautomerase, DCT), eumelanin synthesis, and the number of stage IV melanosomes markedly decreased in *ru2^{d}/ru2^{d}* melanocytes. However, excess L-tyrosine (Tyr) added to culture media from initiation of the primary culture rescued the reduced differentiation through increase in TYR activity, expression of TYR, TRP1, TRP2 and Kit, eumelanin synthesis, and stage IV melanosomes. L-Tyr injected into *ru2^{d}/ru2^{d}* mice also stimulated melanocyte differentiation. These results suggest that the *ru2^{d}* allele inhibits melanocyte differentiation, and that its impaired differentiation is rescued by excess Tyr.

Key words: ruby-eye, Hermansky-Pudlak syndrome, melanocyte, tyrosinase, melanosome

INTRODUCTION

The pigment-producing cells, melanocytes, are derived from the neural crest, a pluripotent embryonic cell population (Rawles, 1947). Their precursors, melanoblasts, invade and colonize the epidermis (Mayer, 1973). Mouse epidermal melanocytes are known to differentiate from melanoblasts at around the time of birth (Hirobe, 1984). The proliferation and differentiation of melanocytes during development are regulated by genetic and epigenetic factors (Hirobe, 1992a). The coat color genes are important genetic factors (Silvers, 1979; Hirobe, 1992a, 2011; Hirobe and Abe, 1999; Bennett and Lamoreux, 2003; Lamoreux et al., 2010). In mice, more than 300 genes are involved in melanocyte proliferation and differentiation, and about a half of these genes have been cloned and their functions clarified. However, many unknown genes and their functions remain to be investigated.

Melanin synthesis is mainly controlled by three melanogenic enzymes, namely tyrosinase (TYR), TYR-related protein 1 (TRP1) and TRP2 (Hearing, 2000; Ito, 2003). TYR initiates melanin synthesis by catalyzing oxidation of L-tyrosine (Tyr) to dopaquinone (Cooksey et al., 1997). TRP1 possesses 5,6-dihydroxyindole-2-carboxylic acid (DHICA)-oxidase activity (Jackson et al., 1990). In contrast, TRP2 possesses dopachrome tautomerase (DCT) activity (Jackson et al., 1992; Tsukamoto et al., 1992) that converts

* Corresponding author. Phone: +81-43-206-3253;
Fax : +81-43-206-4638;
E-mail: thirobe@nirs.go.jp
doi:10.2108/zsj.28.790

dopachrome (DC) to DHICA (Korner and Pawelek, 1980). Melanocytes produce two types of melanin: brownish-black eumelanin and reddish-yellow pheomelanin (Ito, 2003). Although differences exist in molecular sizes and general properties, these melanins arise from a common metabolic pathway in which dopaquinone is a key intermediate (Hearing and Tsukamoto, 1991; Ito and Wakamatsu, 2008).

In 2006, a spontaneous mutant of brown coat color with ruby eyes occurred in offspring of a C57BL/10JHir (B10; black) mouse dam (Hirobe, 2011). The phenotype of this mutant was similar to that of ruby-eye (*ru*/*Hps6*^{ru}) or ruby-eye 2 (*ru2*/*Hps5*^{ru2}) (Silvers, 1979). Human HPS is a recessively inherited disease that affects several organs, such as the skin (hypopigmenation), eyes (low visual acuity), blood cells (prolonged bleeding), and lung (interstitial pulmonary fibrosis) (Wei, 2006). Many distinct types of human HPS have been described to date (Wei, 2006). In mice, many naturally occurring hypopigmentation models of HPS have been characterized (Wei, 2006). Human *HPS5* corresponds to mouse *Hps5*^{ru2} (*ru2*), and *HPS6* to *Hps6*^{ru} (*ru*) (Zhang et al., 2003). To clarify whether our mutant corresponds to the *Hps6* or *Hps5* gene, reverse transcription-polymerase chain reaction (RT-PCR) analysis was performed in black and mutant mice. Moreover, to understand the role of this mutant gene in the regulation of the proliferation and differentiation of melanocytes, melanocytes in serum-free primary cultures were studied.

MATERIALS AND METHODS

Mice

All animals used in this study were strain B10-+/+ and its spontaneous mutant, B10-*ru2*^{d}/*ru2*^{d} (*Hps5*$^{ru2\text{-}d}$/*Hps5*$^{ru2\text{-}d}$) (congenic) of the house mouse, *Mus musculus*. The B10-*ru2*^{d}/*ru2*^{d} congenic strain was a descendant of one pair (♀ 1: ♂ 1) from three ruby-eye-like mutants (♀ 1: ♂ 2) that occurred in B10 mice in 2006. Mice were given water and a commercial diet, OA-2 (Clea Japan, Tokyo, Japan) ad libitum. They were maintained at 24 ± 1°C with 40–60% relative humidity: 12 hours of fluorescent light were provided daily. The present study was approved by the ethics committee of the National Institute of Radiological Sciences in accordance with the guidelines of the National Institutes of Health.

RT-PCR analysis and cDNA and genomic sequencing

Tail skins were excised from 5-week-old black and mutant mice, as well as their F_1 and F_2 progeny, and stored at –80°C before use. Total RNAs were extracted using a TRIzol Plus RNA Purification kit (Invitrogen, Carlsbad, CA, USA) and any contaminating genomic DNA was removed by DNase1 treatment (Invitrogen, 15 minutes at 25°C). Next, 3 mg of each of DNA-free total RNAs were then reverse transcribed using a ThermoScript™ RT-PCR system (Invitrogen) according to the manufacturer's directions, and the template RNAs were removed from the newly synthesized cDNA by RNase H digestion (Invitrogen; 20 minutes at 37°C).

To sequence the full length of mRNAs for mouse *Hps6* and *Hps5* genes, one-tenth aliquot of the cDNA was amplified in the presence of several oligonucleotide primer sets specific for each gene, which were designed based on the reported sequences (Table 1). PCR reactions were performed using Platinum Taq DNA polymerase (Invitrogen) and a Thermal Cycler (i-cycler; Bio-Rad Laboratories, Inc., DriveHercules, CA, USA). After activation of DNA polymerase by incubating for two minutes at 94°C, 42 cycles of reactions including denaturation for 30 seconds at 94°C and annealing/extension for one minute at 60°C were performed, followed by additional extension for 10 minutes at 72°C.

The amplified cDNAs were purified using a NucleoSpin Extract II (MACHEREY-NAGEL GmbH & Co. KG, Düren, Germany) according to the manufacturer's directions, followed by direct sequencing using gene specific primers, an ABI PRISM BigDye Terminator Cycle Sequencing Ready Reaction kit (Applied Biosystems, Foster City, CA, USA) and an automatic sequencer (ABI PRISM 310 Genetic Analyzer; Applied Biosystems). Primers used for sequencing of Hps5 and Hps6 cDNAs are shown in Table 1.

To analyze the expression of mRNAs for mouse *Hps5* genes, one-tenth aliquot of the cDNA was amplified using primer sets shown in Table 1 as described above. One-tenth aliquot of each reaction was electrophoresed on 2% agarose gels, stained with etidium bromide, and photographed under ultraviolet illumination. The amplified DNA fragments were recovered from the gels and purified using NucleoSpin Extract II, and then subjected to direct sequencing using Hps5-f4 as described above. Genomic DNA was extracted using SimplePrep™ reagent for DNA (Invitrogen). To sequence intron 9 and exon 10 of Hps5, genomic DNA was amplified using primer sets (Table 1) as described above. Purification of amplified DNA was performed as described above. Sequencing of Hps5 genomic DNA was performed using the same methods as described above.

Table 1. Sequence of primer sets used.

NCBI Reference Sequence	Name of primer	Sequence	Position
(A) Forward			
NM_001005247.2	Hps5-f1	gcagcgcctccagggcctaga	575–595
	Hps5-f4	aatctcacatctttccctgttgtctgt	1692–1718
	Hps5-f7	ctggcttgtcgtttcctaaagaagta	2959–2984
	Hps5-f2	agaacacaaaggccgaaaagttactg	1005–1030
	Hps5-f3	aactttgacggggaagtgctcagta	1393–1417
	Hps5-f5	gcagggctgtggtgccaatagga	2130–2152
	Hps5-f6	ggtgctaagaatggttttacttgagt	2554–2569
	Hps5-f8	cttgagttccttctacaaccagagt	3367–3391
	Hps5-f9	cataagcctgatggaaggggacaatg	3672–3697
	Hps5-ex9-F	agtgaacactgtgtgctgacttgga	1543–1567
NC_000073.5	Hps5intron9-f1	tttagtcaagacagatacctcttcatg	
	Hps5intron9-f2	tgattatagcccgtgtcaaaatggta	
NM_176785.3	Hps6-f1-2	cccgggtaccaggactagcagt	41–62
	Hps6-f4	agacccgaggagccctacgat	1227–1247
	Hps6-f2	aggtttggggcgtggggatgga	423–444
	Hps6-f3	tccatctcttggtctttcacacagta	808–833
	Hps6-f5	acaccattttccaagcccttcctaca	1638–1663
	Hps6-f6	gctacaagctgtaaggcagctgat	2026–2049
	Hps6-f7	ctgctagaacagactggggctcaa	2330–2353
(B) Reverse			
NM_001005247.2	Hps5-r1	caaatgctccaacttatctgcagtcaa	1825–1851
	Hps5-r2	gctccgtgtaggcaggattagatctt	3087–3112
	Hps5-r3	agggtcgagagcaggattccactt	4049–4072
NM_176785.3	Hps5-ex10-R	gccaggtcccacaggcctctcctt	1743–1766
	Hps6-r1	gaaggctccgacgctggtagt	1347–1367
	Hps6-r2	acaagtcccaccttcgtgctt	2575–2595

Melanocyte primary culture

The method for serum-free primary culture of melanoblasts and melanocytes from 0.5-day-old mice was reported previously (Hirobe, 1992b). Briefly, disaggregated epidermal cell suspensions were pelleted by centrifugation and suspended in Ham's F-10 medium (Gibco, Grand Island, NY, USA). The cell pellet after centrifugation was resuspended in culture media. Unless stated otherwise, all reagents were purchased from Sigma Chemical Co. (St. Louis, MO, USA). Four kinds of culture media were used: melanoblast-defined medium (MDM) consisting of F-10 plus 10 μg/ml insulin (bovine), 0.5 mg/ml bovine serum albumin (Fraction V), 1 μM ethanolamine, 1 μM phosphoethanolamine, 10 nM sodium selenite, 100 U/ml penicillin G, 100 μg/ml streptomycin sulfate, 50 μg/ml gentamicin sulfate and 0.25 μg/ml amphotericin B; melanocyte-differentiation medium (MDMM) consisting of MDM supplemented with 100 nM α-melanocyte-stimulating hormone (MSH); melanocyte-proliferation medium (MDMD) consisting of MDM supplemented with 0.5 mM dibutyryl adenosine 3':5'-cyclic monophosphate (DBcAMP); and, melanoblast-proliferation medium (MDMDF) consisting of MDMD supplemented with 2.5 ng/ml basic fibroblast growth factor (bFGF) (Invitrogen). Cells in each epidermal cell suspension were counted in a hemocytometer chamber and plated onto type I collagen (Becton Dickinson, Bedford, MA, USA)-coated dishes at an initial density of 1×10^6 cells/35 mm dish (1.04×10^5 cells/cm^2). Cultures were incubated at 37°C in a humidified atmosphere of 5% CO_2 and 95% air (pH 7.2). The medium was replaced with fresh medium four times a week. After 14 days, pure cultures of melanoblasts or melanocytes were obtained. In some cases, additional L-tyrosine (Tyr) was added to MDMD from 0.1 to 2 mM from initiation of the primary culture. The standard concentration of L-Tyr included in Ham's F-10 is 10 μM. The same lots of these reagents were used in this study.

Assays for proliferation and differentiation

The method for counting the number of melanoblasts and melanocytes was reported previously (Hirobe, 1992b). It is known that L-3,4-dihydroxyphenylalanine (dopa) reaction detects TYR-containing melanocytes, and combined dopa-premelanin reaction (ammoniacal silver nitrate staining after the dopa reaction) detects stage I and II melanosome-containing melanoblasts in addition to differentiated melanocytes (Hirobe, 1992b). Melanoblasts were also stained by antibodies to TRP1 and TRP2 (Hirobe et al., 2002). A melanoblast is defined here as an unpigmented cell that possesses no TYR activity.

Immunocytochemical staining

Cells cultured for seven days were fixed with chilled 95% ethanol for 1.25 min (for polyclonal antibodies) or 1.5 min (for monoclonal antibodies). The cells were treated with normal goat serum (KPL, Gaithersburg, MD) for 15 min at room temperature (RT). For Kit staining, the cells were treated with ACK2 (a rat anti-mouse Kit antibody kindly supplied by Dr. Nishikawa, RIKEN, Kobe, Japan) or normal rat immunoglobulin G2b (20 μg/ml; PharMingen, San Diego, CA, USA) as a negative control for 1 hr at RT. The cells were then reacted with alkaline phosphatase-labeled anti-rat IgG (at 100× dilution; Southern Biotechnology Associates, Birmingham, LA, USA) for 1 hr at RT. For the staining of TYR, TRP1 and TRP2, the cells were treated with anti-PEP7, PEP1, and PEP8 (at 500× dilution; kindly supplied by Dr. Hearing, NIH, Bethesda, MD, USA) overnight at 4°C. Normal rabbit serum (at 500× dilution; DAKO, Carpinteria, CA, USA) and IgG of normal rabbit serum were used as negative controls. The cells were then reacted with alkaline

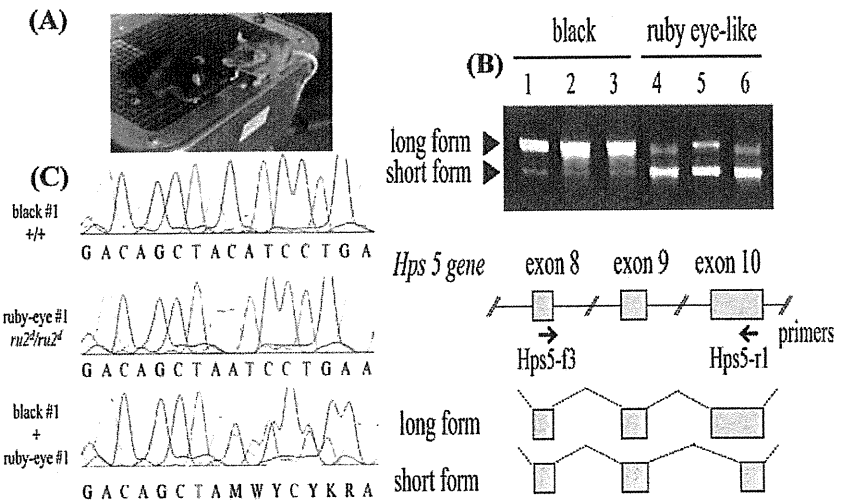

Fig. 1. Pictures of black (B10-+/+; left; black coat and black eyes) and ruby-eye-like mutant (B10-*ru2^d/ru2^d*; right; brown coat and ruby eyes) mice (**A**), RT-PCR analysis of product of the *Hps5* gene (**B**) and sequence analysis data (**C**). (**B**) *Hps5* expression was detected by RT-PCR in tail skins of three blacks and three ruby-eye-like mutants, and diagram of isoform (long form and short form) of the *Hps5* gene. (**C**) Sequence data of amplified gene fragment of black, ruby-eye-like mutant and their 1:1 mixture are shown. As the intron just before the exon 10 possessed a repetitive A sequence, we were unable to determine the genomic DNA sequence by using forward primers, thus we determined its sequence by using reverse primers prepared in exon 10. The DNA sequence is shown as a reverse sequence. R (A/G), Y (C/T), K (G/T), M (A/C), W (A/T).

Table 2. Segregation of the type of coat color and eyes of offspring in the F_1, F_2 and backcross generations from crosses between B10 and ruby-eye-like mutant. Type of coat color and eye color was observed in the F_1, F_2 and backcross generations from crosses between B10 and mutant 25 days after birth. Coat color and eye color were completely coincident, namely black coat mice possessed black eyes and ruby-eye-like mice possessed brown coat and ruby eyes.

Generation	Black	Ruby-eye-like	χ^2	P
P	56 (♀ 25, ♂ 31)			
P		59 (♀ 31, ♂ 28)		
F_1 (B10 ♀ × mutant ♂)	43 (♀ 21, ♂ 22)			
F_1 (mutant ♀ × B10 ♂)	41 (♀ 18, ♂ 23)			
F_2 (B10 ♀ × mutant ♂)	27 (♀ 13, ♂ 14)	11 (♀ 5, ♂ 6)		
Exp. (3:1)	28.5	9.5	0.12	$0.70 < P < 0.80$
F_2 (mutant ♀ × B10 ♂)	52 (♀ 25, ♂ 27)	23 (♀ 11, ♂ 12)		
Exp. (3:1)	50	25	0.14	$0.70 < P < 0.80$
BC (B10 ♀ × F_1 ♂)	55 (♀ 24, ♂ 31)			
BC (F1 ♀ × B10 ♂)	62 (♀ 28, ♂ 34)			
BC (mutant ♀ × F_1 ♂)	41 (♀ 25, ♂ 16)	29 (♀ 13, ♂ 16)		
Exp. (1:1)	35	35	1.73	$0.10 < P < 0.20$
BC (F_1 ♀ × mutant ♂)	39 (♀ 25, ♂ 14)	44 (♀ 23, ♂ 21)		
Exp. (1:1)	41.5	41.5	0.19	$0.50 < P < 0.70$

phosphatase-labeled anti-rabbit IgG (at 100× dilution; DAKO) for 1 hr at RT. Colorization was developed using the new fuchsin substrate system (DAKO) and levamisole solution (Vector, Burlingame, CA, USA) as an inhibitor of internal alkaline phosphatase (Kawa et al., 2000).

Assays of eumelanin and pheomelanin

Eumelanin and pheomelanin were assayed as specific degradation products pyrrole-2,3,5-tricarboxylic acid (PTCA) and 4-amino-3-hydroxyphenylalanine (4-AHP) after permanganate oxidation and hydroiodic acid hydrolysis, respectively (Ito and Fujita, 1985; Ito and Wakamatsu, 1994; Ozeki et al., 1995; Wakamatsu et al., 2002). Epidermal cell suspensions were cultured in MDMD for 12 days. At this stage, cultures consisted of mostly pure melanoblasts and melanocytes. They were then provided with 1 ml of fresh MDMD. The cells were incubated for another two days, and the resulting conditioned media from multiple paired dishes (10–20) were collected with a Pasteur pipette and stored in plastic centrifuge tubes (Becton Dickinson) at –80°C. At the same time, melanocytes cultured for 14 days were harvested with a solution of 0.05% trypsin (Difco, Sparks, MD, USA) and 0.02% ethylenediaminetetraacetate (EDTA) in calcium- and magnesium-free phosphate buffered saline at 37°C for 10 min. After trypsinization was inhibited by the addition of 2000 U/ml of soybean trypsin inhibitor, cell pellets were collected by centrifugation. Collected cells and cultured media were processed to analysis of PTCA and 4-AHP by the methods reported previously (Hirobe et al., 1998).

Electron microscopy

Pure primary melanoblasts and melanocytes cultured for 14 days in MDMD with or without L-Tyr were treated with trypsin and EDTA similarly, and all cell pellets were fixed in chilled 2.5% glutaraldehyde (Wako, Osaka, Japan) solution in 0.1 M phosphate buffer, pH 7.4. After washing with chilled 0.1 M phosphate buffer, cells were postfixed in chilled 1% osmium teroxide (Taab Laboratories Equipment Ltd., Berkshire, UK) in 0.1 M phosphate buffer (Hirobe and Abe, 2007). After washing with chilled 0.1 M phosphate buffer, the cells were dehydrated in a series of graded ethanols and embedded in epoxy resin (Taab Laboratories Equipment Ltd.). Ultrathin sections were cut with a diamond knife on an ultramicrotome (Reichert Ultracuts, Leica, Heerbrugg, Switzerland), stained with uranyl acetate and lead citrate, and examined with a transmission electron microscope (IEM-1210, Jeol, Tokyo, Japan). Electron micrographs of +/+ melanocytes (control = 41, L-Tyr = 42 figures) as well as $ru2^d/ru2^d$ melanocytes (control = 45, L-Tyr = 46 figures) were surveyed on the presence of stage I, II, III, and IV melanosomes (Fitzpatrick et al., 1969), the Golgi apparatus, mitochondria and lysosomes, and calculated per unit area (100 μm^2). The total number of melanosomes present in +/+ melanocytes counted was 2486 for control cells and 2998 for L-Tyr-treated cells, and of melanosomes present in $ru2^d/ru2^d$ melanocytes was 1115 for control cells and 2192 for L-Tyr-treated cells, respectively. To investigate quantitatively the effect of the mutation as well as of L-Tyr on the ultrastructure of melanosomes, the number of melanosomes in each stage of development was scored. By scoring the number of melanosomes in each stage, it is possible to determine the degree of melanocyte differentiation.

Effects of L-Tyr in vivo

L-Tyr (1 mM in 0.9% NaCl solution, 0.1 ml/gBW) was injected subcutaneously to the dorsal skin of +/+ and $ru2^d/ru2^d$ mice everyday starting 0.5 days after birth and its effects on the proliferation and differentiation of melanocytes were studied. Each experimental and control group consisted of three mice. Skin samples were fixed at 6.5 days in 16% formalin in phosphate buffer and washed with distilled water and incubated with

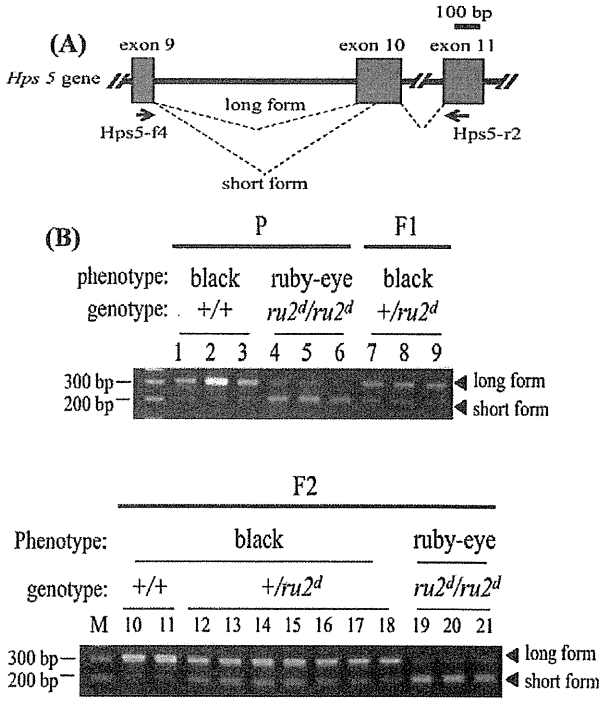

Fig. 2. Structure of the *Hps5* gene and its expression. (**A**) Structure of the *Hps5* gene and primers for RT-PCR analysis. RT-PCR analysis using primer (Hps5-f4) located in exon 9 and primer (Hps5-r2) located in exon 11 can detect both mRNA of long form and short form. (**B**) RT-PCR analysis of expression of the *Hps5* gene. Electrophoresis patterns of reaction products using primers.

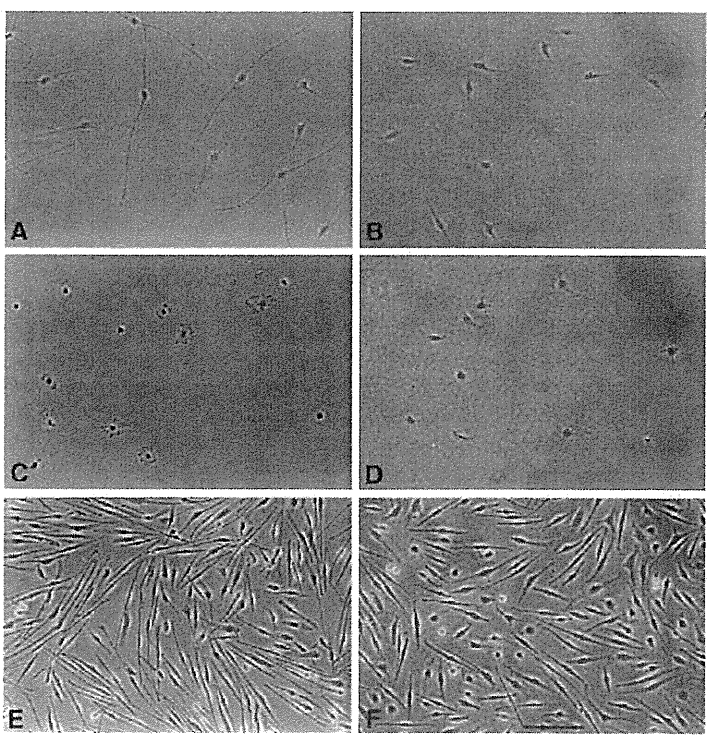

Fig. 3. Melanoblasts and melanocytes in pure cultures derived from epidermal cell suspensions of 0.5-day-old +/+ (**A**, **C**, **E**) and $ru2^d/ru2^d$ (**B**, **D**, **F**) cultured for 14 days in MDM (**A**, **B**), MDMM (**C**, **D**) and MDMDF (**E**, **F**). Undifferentiated $ru2^d/ru2^d$ melanoblasts (**B**, **D**, **F**) are less dendritic than are +/+ melanoblasts (**A**, **E**) or melanocytes (**C**). Phase-contrast microscopy. Scale bar, 100 μm.

0.1% L-dopa solution in phosphate buffer (pH 7.4) for 16–18 hours at 37°C. After the dopa reaction, skin samples were processed to paraffin sections (10 μm thick), and stained with ammoniacal silver nitrate solution (combined dopa-premelanin reaction). The sections were counterstained with eosin. The number of melanocytes positive to the dopa reaction as well as the number of melanoblasts and melanocytes positive to the combined dopa-premelanin reaction was counted per 0.1 mm^2 of the interfollicular epidermis.

Statistics

Calculations of genetic ratios were made from chi-square (χ^2) analysis. In calculations of values of χ^2, actual number observed and those expected were used. The statistical significance of differences in the number of melanoblasts/melanocytes, in the percentage of melanocytes in the melanoblast-melanocyte population, in the number of melanosomes, the Golgi apparatus, mitochondria and lysosomes, in eumelanin and pheomelanin contents and in the number of melanocytes and melanoblasts/melanocytes in vivo between control and experiment was determined by Student's *t*-test (two-tailed).

RESULTS

Genetic analysis of ruby-eye-like mutation

All the offspring from reciprocal F_1 crosses between black mice (Fig. 1A left) and mutant mice (Fig. 1A right) had a black coat with black eyes. In the reciprocal F_2, 3:1 ratios of segregation of coat and eyes were observed (Table 2). In the reciprocal backcross of F_1 with black mice, all exhibited black coat and black eyes (Table 2). In the reciprocal backcross of F_1 with mutant mice, ratios of 1:1 of segregation of coat and eyes were observed (Table 2). These results suggest that the ruby-eye-like mutation is regulated by a single autosomal recessive gene.

Sequence analysis of the *Hps6* gene in mutant showed no difference between black and mutant. RT-PCR analysis of the *Hps5* gene revealed two kinds of amplified cDNAs (Fig. 1B). One is long form that has already been known, and the other is novel short form. The long form contained open reading frame (ORF) coding 1126 amino acids (aa). In contrast, the short form cDNA was devoid of 99 bases and 33 aa. The deleted base sequence was ATATTCAGGATGTAGCTGT CTACAAGAATGAATTGTTC TGTTTACACTTTAATGGAA AAATCTCACATCTTTCCCT GTTGTCTGTGGAGCGCTG TGTAG, and the aa sequence was DIQDVAVYKNELFCLHFNGKISHLSLLSVERCV. Thus, the short form contained ORF coding 1083 aa. This may be caused by the connection of exon 9 with the splicing acceptor site of exon 10 (at position of 1085, 99 base pair downstream from 986). The long form was predominant in black mice, while the short form in mutant mice.

Sequence analysis of full-length cDNA of the long form and genomic DNA revealed that 997G (the translation initiation site (ATG) is defined as nucleotide number 1) was deleted in mutant mice. Although the 997G deletion caused a frame shift mutation, the first codon was a stop codon (TAG, 997–999). There was no difference in the sequence of the short form between black and mutant mice, since this deletion site (*Δ*G997) of exon10 was not included in the short form (Fig. 1B). From these results, we designated this novel mutant allele *ru2*^{d} (*Hps5*$^{ru2\text{-}d}$).

Using primers inside exons 8 and 10 of the *Hps5* gene (Fig. 1B), genomic DNAs of black and mutant mice were used as the templates for PCR. The sequence of the gene fragment (about 1100 bp) of the *Hps5* gene was determined using primers inside exon 10. The sequence of black mice was GACAGCTACATCCTGA (C: deletion site), while that of mutant mice was GACAGCTAATCCTGAA. 1:1 mixture of DNA samples of black and mutant mice showed that two bases were overlapped from the deletion site (Fig. 1C).

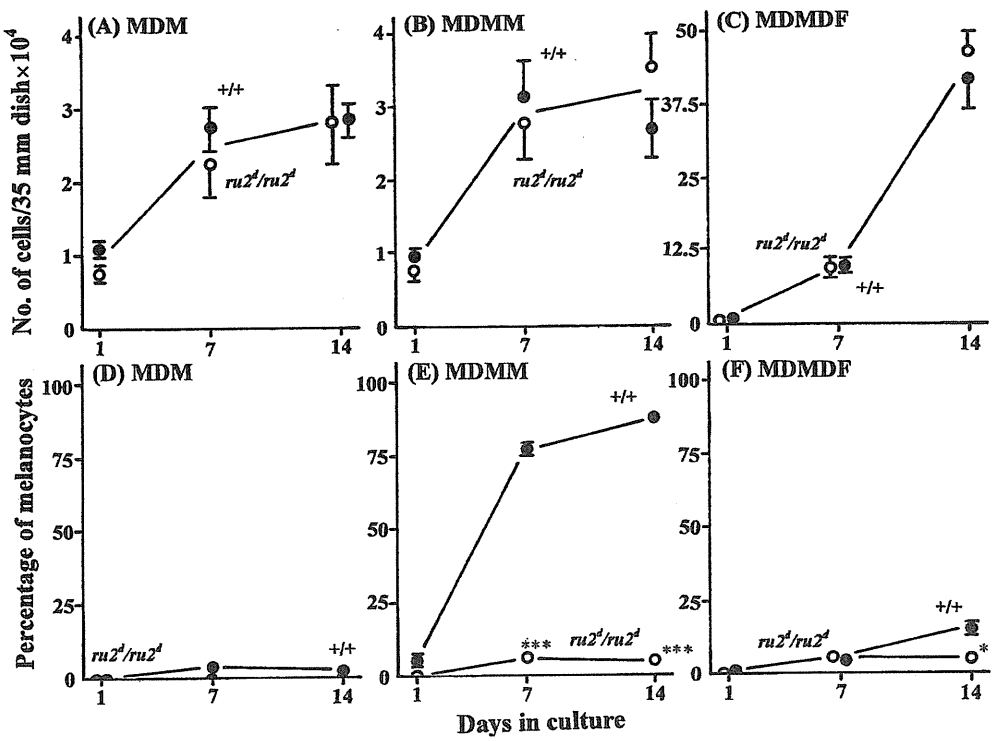

Fig. 4. Kinetics of the proliferation (**A–C**) and differentiation (**D–F**) of epidermal melanoblasts and melanocytes from 0.5-day-old +/+ (●) and *ru2*^{d}/*ru2*^{d} (○) in MDM (**A, D**), MDMM (**B, E**) and MDMDF (**C, F**). Epidermal cell suspensions were cultured for 14 days. The number of melanoblasts and melanocytes was counted at 1, 7 and 14 days. The number of *ru2*^{d}/*ru2*^{d} melanoblasts and melanocytes did not differ from that of +/+ cells, whereas the percentage of differentiated melanocytes in *ru2*^{d}/*ru2*^{d} cultured in MDMM and MDMDF was much lower than in +/+. The data are averages of results from four experiments. Each experiment was performed with different litters of mice. Bars indicate standard error of the mean (SEM), and are shown only when they were larger than symbols. Statistically significant differences (*$P < 0.05$, **$P < 0.01$, ***$P < 0.001$).